


Internal energy balance and aerodynamic heating predictions for hypersonic turbulent boundary layers

Matthew Barone ^{*}

Aerosciences Department, Sandia National Laboratories, Albuquerque, New Mexico 87185, USA

Gary L. Nicholson and Lian Duan 

Department of Mechanical and Aerospace Engineering, Ohio State University, Columbus, Ohio 43210, USA



(Received 10 May 2022; accepted 22 July 2022; published 19 August 2022)

The elemental equation governing heat transfer in aerodynamic flows is the internal energy equation. For a boundary layer flow, a double integration of the Reynolds-averaged form of this equation provides an expression of the wall heat flux in terms of the integrated effects, over the boundary layer, of various physical processes: turbulent dissipation, mean dissipation, turbulent heat flux, etc. Recently available direct numerical simulation data for a Mach 11 cold-wall turbulent boundary layer allows a comparison of the exact contributions of these terms in the energy equation to the wall heat flux with their counterparts modeled in the Reynolds-averaged Navier-Stokes (RANS) framework. Various approximations involved in RANS, both closure models as well as approximations involved in adapting incompressible RANS models to a compressible form, are assessed through examination of the internal energy balance. There are a number of potentially problematic assumptions and terms identified through this analysis. The effect of compressibility corrections of the dilatational dissipation type is explored, as is the role of the modeled turbulent dissipation, in the context of wall heat flux predictions. The results indicate several potential avenues for RANS model improvement for hypersonic cold-wall boundary-layer flows.

DOI: [10.1103/PhysRevFluids.7.084604](https://doi.org/10.1103/PhysRevFluids.7.084604)

I. INTRODUCTION

The characterization of turbulent boundary layers in hypersonic conditions has remained an active research area in the study of aerodynamic flows. The practical significance of such efforts is that accurate prediction of aerodynamic heating loads remains a challenging and important topic in hypersonic vehicle design. This article addresses methods for predicting steady-state heating when the boundary layer is fully turbulent and the wall temperature, T_w , is significantly lower than the adiabatic recovery temperature, T_r (i.e., cold-wall conditions). Models based on the Reynolds-averaged Navier-Stokes (RANS) equations continue to be widely used for design and analysis under such conditions. As is well known, most RANS models were originally developed for low-speed/incompressible flow, and then extended to compressible flow with typically modest modifications. Such an approach is justified by the substantial amount of evidence from experiments and direct numerical simulations that indicates that wall-bounded turbulence is essentially incompressible in nature well into the hypersonic regime, with the effects of compressibility being felt primarily through variations in mean density and temperature [1]. This approach has been largely successful for relatively simple supersonic and hypersonic flow configurations involving

*mbarone@sandia.gov

attached flow in the presence of mild pressure gradients and with moderate heat transfer. However, for hypersonic cold-wall flows, accurate prediction of wall heat flux for turbulent boundary layers has been inconsistently achieved by many RANS models.

Various previous works have considered the validation of RANS models for prediction of aerodynamic heating in hypersonic flow. MacLean *et al.* [2] compared RANS solutions to surface heat flux measurements obtained from the HIFiRE-1 ground test campaign. The HIFiRE geometry consisted of a conical forebody with cylindrical afterbody, and the validation assessment included data for the forebody with fully turbulent boundary layer. Calculations at free stream Mach numbers of 6.6 and 7.2 were made, with cold-wall surface conditions. The one- and two-equation RANS models that were tested tended to overpredict wall heat flux, while an algebraic model (Baldwin-Lomax) gave the best results. The authors noted that they considered only cases for the HIFiRE trajectory nominal conditions near Mach 7, but that they also measured other test articles at higher Mach number conditions, and results showed some cases where the error in the predictions became worse at higher speeds. Predictions of a k - ω turbulence model gave similar overpredictions compared to measured wall heat flux on the HIFiRE-1 flight test at Mach 5.1 [3]. Gnoffo *et al.* [4] included a Mach 11 cold-wall flat-plate case in their assessment of RANS models for hypersonic re-entry flows. Popular one- and two-equation RANS models overpredicted the wall heat flux for this case by as much as 35%, while algebraic models performed better; similar findings and assessment of RANS solutions versus direct numerical simulation (DNS) for this flow were reported in Huang *et al.* [5]. Aiken *et al.* [6] studied the performance of three RANS models for predicting mean velocity profile, mean temperature profile, wall shear stress, and wall heat flux for a variety of compressible turbulent boundary layers, including cold-wall boundary layers, up to Mach 14 (and including the Mach 11 case mentioned above). They found that none of the models accurately predicted wall shear stress or heat flux (in comparison to DNS) for the Mach 11 and Mach 14 cases, and that errors in these quantities increased with increasing Reynolds number. More accurate heat flux predictions can be made by applying compressibility corrections to the two-equation models, but often at the expense of worsening agreement with measured wall shear stress [4,7] and/or temperature profile [6]. A number of papers have demonstrated good predictions of hypersonic, cold-wall heat flux for simple flow configurations using algebraic turbulence models [5,8–10]. However, algebraic models do not generalize to more complicated geometries and flow topologies as readily as transport equation-based models, and thus the latter are often used for vehicle design and analysis. The agreement of RANS models with experimental measurements and DNS certainly depends upon the particular flow conditions and models considered. For example, Huang *et al.* [11] showed decent agreement between several RANS models and DNS of a Mach 8 turbulent boundary layer with wall-to-recovery temperature ratio of 0.48 at relatively low Reynolds numbers. Nonetheless, to date, there has been little analysis available to explain the uneven performance of this class of models on simple flat plate and conical flows. The present work aims to address this gap by elucidating problematic turbulence modeling strategies and assumptions, so that these can be improved upon in future versions of turbulence models for hypersonic flow.

Our approach is to examine RANS model formulations and their predictions of wall heat flux using integral expressions relating terms in the internal energy equation to the wall heat flux. Similar expressions were originally derived by Fukagata *et al.* [12] for decomposition of wall shear stress into integral term contributions for incompressible plane channel, pipe, and boundary-layer flows. This class of integral expressions is often referred to in the literature as a Fukagata-Iwamoto-Kasagi (FIK) decomposition. Gomez *et al.* [13] extended the analysis of wall shear stress to compressible plane channel and boundary-layer flows, identifying a “compressible” term associated with temperature-dependent viscosity and a “compressible-turbulent interaction” term associated with correlation of viscosity-strain fluctuations; see also Ref. [14] for further extensions and application of this decomposition. Fukagata *et al.* [15] derived an expression for the contribution of the turbulent heat flux to the wall heat flux for incompressible wall-bounded turbulence. Later, Ebadi *et al.* [16] obtained exact integral expressions for the incompressible wall heat flux that contain no explicit

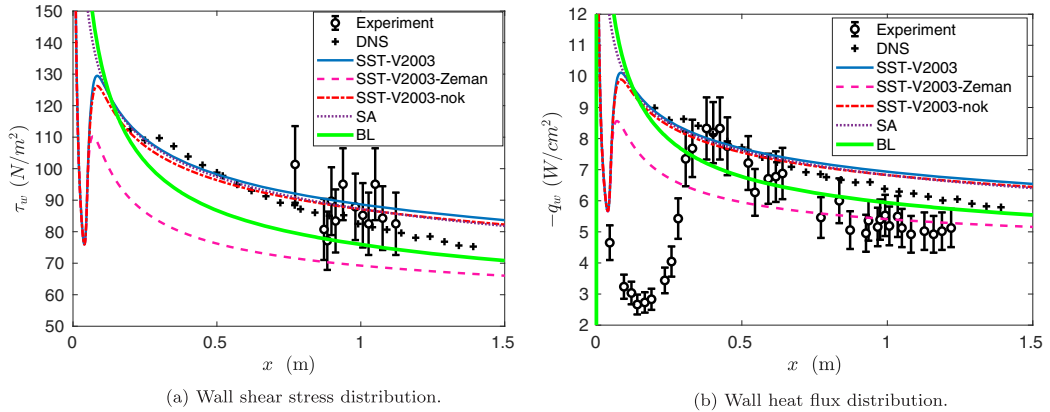


FIG. 1. Comparisons of RANS model results with DNS and experimental data for Mach 11 flat-plate turbulent boundary layer.

stream-wise gradient terms. Zhang and Xia [17] utilized the internal energy equation to derive integral expressions for the wall heat flux for *compressible* isothermal-wall plane channel flow. They found that the mean viscous dissipation gave the largest contribution to the wall heat flux for Mach numbers of 0.5, 1.5, and 3.0, while turbulent dissipation was also found to be a significant contributor; the contribution of the turbulent heat flux was modest and comparable to that of the molecular heat flux. Wenzel *et al.* [18] utilized the momentum and total enthalpy boundary layer equations to derive FIK-style integral relationships that were subsequently used to assess effects of compressibility, pressure gradient, and heat transfer on subsonic to low-supersonic turbulent boundary layers.

In the present work, we consider a turbulent flat-plate boundary layer at a nominal free stream Mach number of 11, and with a cold wall ($T_w/T_r = 0.20$), for which DNS results [19], as well as experimental measurements of wall shear stress and wall heat flux [4], are available. Figure 1 compares wall shear stress and wall heat flux distributions between experiment, DNS, and the RANS results from the present work. For wall shear stress, reasonable agreement is observed between experiment, DNS, and RANS, given the level of uncertainty in the measurements. The RANS models give a rather broad range of predictions, with the lowest values given by the SST model with Zeman compressibility correction, where wall shear appears to be underpredicted. Notably, the slope of the RANS model predictions with increasing stream-wise distance is shallower than that of the DNS distribution. For wall heat flux, some discrepancy between experiment and DNS is observed. For larger values of stream-wise distance x (and, hence, larger Reynolds number), the discrepancy appears as a bias, with DNS and experiment showing similar slopes of the distribution. The RANS results without the compressibility correction give a shallower slope for larger x and overpredict both the DNS and the experimental measurements. Relative to the DNS, the wall heat flux is overpredicted by more than 10% for the largest Reynolds number, with the prediction error increasing with increasing Reynolds number. For this canonical flow, it is desirable to reduce this error and to employ models with correct Reynolds number dependence of the wall heat flux. Failure of models to capture correct dependence of wall heat flux on Reynolds number may lead to larger errors for predictions on flight vehicles, where Reynolds number may exceed levels typically achieved in validation experiments conducted in wind tunnel facilities.

The main contribution of this work is to utilize the internal energy equation to compare the integrated wall heat flux budgets between RANS and DNS, and to explain how the RANS model and resulting solutions lead to predictions of surface heat flux. The perspective and methods used here are similar to those of Pond *et al.* [20], who used integral FIK relations for wall shear stress

and heat flux to validate RANS models for prediction of reciprocating, nonisothermal channel flow. The present analysis provides a connection, heretofore unavailable, between RANS model forms, resulting solution fields, and the generated surface heat flux prediction for cold-wall hypersonic turbulent boundary layers.

In Sec. II, we present the exact averaged internal energy equation as well as implied forms of this equation solved by some common RANS models. In Sec. III, we derive the double-integrated internal energy equation, which provides a decomposition of the wall heat flux for a spatially developing compressible turbulent boundary layer. Section IV describes the RANS models evaluated later in this paper. Section V describes the DNS data set and examines the heat flux budget given by the DNS solution. Section VI presents comparisons between the DNS and RANS models using the integral relations from Sec. III. The implications of the results for turbulence modeling strategies are discussed in Sec. VII, with conclusions given in Sec. VIII.

II. INTERNAL ENERGY EQUATIONS

A. Evolution equation for internal energy

In this section, we present various forms of the internal energy equation for compressible flow of a single-species, nonreacting gas. Total energy is conserved, as expressed in the following equation:

$$\frac{\partial}{\partial t} \left(\rho e + \rho \frac{u_i u_i}{2} \right) + \frac{\partial}{\partial x_j} \left(\rho u_j h + \rho u_j \frac{u_i u_i}{2} \right) = \frac{\partial}{\partial x_j} (u_j t_{ij}) - \frac{\partial q_j}{\partial x_j}. \quad (1)$$

Here, ρ is the density, e is the specific internal energy, u_i is the velocity vector, $h = e + p/\rho$ is the enthalpy with pressure p , and $q_j = -\kappa \frac{\partial T}{\partial x_j}$ is the molecular heat flux vector, with temperature T and thermal conductivity κ . The viscous stress tensor is $t_{ij} = 2\mu S_{ij} - \frac{2}{3}\mu \frac{\partial u_k}{\partial x_k} \delta_{ij}$ where $S_{ij} = \frac{1}{2} \left(\frac{\partial u_i}{\partial x_j} + \frac{\partial u_j}{\partial x_i} \right)$ and μ is the molecular viscosity.

The evolution equation for kinetic energy per unit volume is obtained by taking the dot product of the velocity and the momentum equation, resulting in

$$\frac{\partial}{\partial t} \left(\rho \frac{u_i u_i}{2} \right) + \frac{\partial}{\partial x_j} \left(\rho u_j \frac{u_i u_i}{2} \right) = -\frac{\partial}{\partial x_j} (u_j p) + p \frac{\partial u_j}{\partial x_j} + \frac{\partial}{\partial x_j} (u_j t_{ij}) - t_{ij} \frac{\partial u_i}{\partial x_j}. \quad (2)$$

Taking the difference between (1) and (2) gives the following equation governing the evolution of internal energy:

$$\frac{\partial}{\partial t} (\rho e) + \frac{\partial}{\partial x_j} (\rho u_j e) = -\frac{\partial q_j}{\partial x_j} - p \frac{\partial u_j}{\partial x_j} + t_{ij} \frac{\partial u_i}{\partial x_j}. \quad (3)$$

Note that the definition of enthalpy has been used to combine the pressure flux term in (2), $\frac{\partial}{\partial x_j} (u_j p)$, with the convective flux of enthalpy in (1), $\frac{\partial}{\partial x_j} (\rho u_j h)$, to arrive at the form (3). This point is relevant to modeling considerations discussed in Sec. II C. The left-hand side of (3) is equivalent (after application of mass conservation) to the density times the material derivative of e . The terms on the right-hand side are the divergence of the molecular heat flux, the work due to volumetric expansion or compression, and viscous dissipation, respectively.

B. Exact averaged internal energy equation

For engineering calculations, averaged equations of motion are often used to find solutions for averaged quantities of interest. To this end, we introduce the Favre decomposition for the temperature, internal energy, and velocity fields and the Reynolds decomposition for the pressure and viscous stress. The Favre decomposition of a variable f is $f = \{f\} + f''$, where $\{f\}$ is the density-weighted time or ensemble average of f and f'' is the fluctuation about $\{f\}$. The Reynolds

decomposition is $f = \langle f \rangle + f'$, where $\langle f \rangle$ is the time or ensemble average of f and f' is the fluctuation about $\langle f \rangle$. Taking the Reynolds average of (3) and assuming statistical stationarity of the flow so that the time derivative term is removed lead to

$$\underbrace{\frac{\partial}{\partial x_j} (\langle \rho \rangle \{u_j\} \{e\})}_{\text{Mean Convection}} + \underbrace{\frac{\partial}{\partial x_j} \langle \rho u_j'' e'' \rangle}_{\text{Turbulent Heat Transfer}} = - \underbrace{\frac{\partial \langle q_j \rangle}{\partial x_j}}_{\text{Molecular Heat Transfer}} - \underbrace{\langle p \rangle \frac{\partial \{u_j\}}{\partial x_j}}_{\text{Mean Pressure Dilatation}} - \underbrace{\langle p \rangle \frac{\partial \langle u_j'' \rangle}{\partial x_j}}_{\text{Turbulent Pressure Dilatation}} - \underbrace{\left\langle p' \frac{\partial u_j''}{\partial x_j} \right\rangle}_{\text{Turbulent Pressure Dilatation}} + \underbrace{\langle t_{ij} \rangle \frac{\partial \{u_i\}}{\partial x_j}}_{\text{Mean Dissipation}} + \underbrace{\langle t_{ij} \rangle \frac{\partial \langle u_i'' \rangle}{\partial x_j}}_{\text{Mean Dissipation}} + \underbrace{\left\langle t_{ij}' \frac{\partial u_i''}{\partial x_j} \right\rangle}_{\text{Turbulent Dissipation}}. \quad (4)$$

If the Reynolds decomposition is used for velocity in the pressure-dilatation and dissipation terms, a more succinct form of (4) results:

$$\underbrace{\frac{\partial}{\partial x_j} (\langle \rho \rangle \{u_j\} \{e\})}_{\text{Mean Convection}} + \underbrace{\frac{\partial}{\partial x_j} \langle \rho u_j'' e'' \rangle}_{\text{Turbulent Heat Transfer}} = - \underbrace{\frac{\partial \langle q_j \rangle}{\partial x_j}}_{\text{Molecular Heat Transfer}} - \underbrace{\langle p \rangle \frac{\partial \langle u_j \rangle}{\partial x_j}}_{\text{Mean Pressure Dilatation}} - \underbrace{\left\langle p' \frac{\partial u_j''}{\partial x_j} \right\rangle}_{\text{Turbulent Pressure Dilatation}} + \underbrace{\langle t_{ij} \rangle \frac{\partial \langle u_i \rangle}{\partial x_j}}_{\text{Mean Dissipation}} + \underbrace{\left\langle t_{ij}' \frac{\partial u_i''}{\partial x_j} \right\rangle}_{\text{Turbulent Dissipation}}. \quad (5)$$

In (5), the mean pressure dilatation and mean dissipation contain only Reynolds-averaged terms, and the property $\langle f' g' \rangle = \langle f' g' \rangle$ has been used in the turbulent pressure dilatation and turbulent dissipation terms. The form (4) is consistent with the usual approach in RANS modeling where the Favre-averaged velocity is employed for all terms, highlighting the extra terms involving derivatives of $\langle u_i'' \rangle$ which appear in this context. In (4) and (5), and in the remainder of the paper, we use the abbreviated terminology ‘‘turbulent dissipation’’ to mean ‘‘rate of dissipation of turbulence kinetic energy.’’

C. Approximate averaged energy equations

In this section, we derive the averaged internal energy equation using typical RANS modeling assumptions. Most compressible RANS model implementations solve the conservative form of the governing equations. Therefore, we begin our derivation with the averaged form of the total energy equation (1), again assuming time stationarity:

$$\frac{\partial}{\partial x_j} \left(\langle \rho \rangle \{u_j\} \left[\{h\} + \frac{\{u_i\} \{u_i\}}{2} + \frac{\{u_i'' u_i''\}}{2} \right] \right) + \frac{\partial}{\partial x_j} (\langle \rho \rangle \{u_j'' h''\}) = - \frac{\partial \langle q_j \rangle}{\partial x_j} + \frac{\partial}{\partial x_j} \left(\langle t_{ij} u_i'' \rangle - \langle \rho \rangle \left\{ u_j'' \frac{u_i'' u_i''}{2} \right\} \right) + \frac{\partial}{\partial x_j} (\{u_i\} \langle t_{ij} \rangle - \{u_i\} \langle \rho \rangle \{u_i'' u_j''\}). \quad (6)$$

To derive an equation for Favre-averaged internal energy from (6), we must subtract an equation for the mean component of the Favre-averaged kinetic energy and an equation for the turbulence kinetic energy. The former is derived from the Favre-averaged momentum equation, and can be written as

$$\frac{\partial}{\partial x_j} \left(\langle \rho \rangle \{u_j\} \frac{\{u_i\} \{u_i\}}{2} \right) = - \frac{\partial}{\partial x_j} (\langle p \rangle \{u_j\}) + \langle p \rangle \frac{\partial \{u_j\}}{\partial x_j} + \frac{\partial}{\partial x_j} (\{u_i\} \langle t_{ij} \rangle) - \langle t_{ij} \rangle \frac{\partial \{u_i\}}{\partial x_j} - \frac{\partial}{\partial x_j} (\langle \rho \rangle \{u_i\} \{u_i'' u_j''\}) + \langle \rho \rangle \{u_i'' u_j''\} \frac{\partial \{u_i\}}{\partial x_j}. \quad (7)$$

Subtracting (7) from (6) gives

$$\begin{aligned} & \frac{\partial}{\partial x_j} \left(\langle \rho \rangle \{u_j\} \left[\{h\} + \frac{\{u_i'' u_i''\}}{2} \right] \right) + \frac{\partial}{\partial x_j} (\langle \rho \rangle \{u_j'' h''\}) \\ &= -\frac{\partial \langle q_j \rangle}{\partial x_j} + \frac{\partial}{\partial x_j} \left(\langle t_{ij} u_i'' \rangle - \langle \rho \rangle \left\{ u_j'' \frac{u_i'' u_i''}{2} \right\} \right) + \frac{\partial}{\partial x_j} (\langle p \rangle \{u_j\}) \\ & \quad - \langle p \rangle \frac{\partial \{u_j\}}{\partial x_j} + \langle t_{ij} \rangle \frac{\partial \{u_i\}}{\partial x_j} - \langle \rho \rangle \{u_i'' u_j''\} \frac{\partial \{u_i\}}{\partial x_j}. \end{aligned} \quad (8)$$

Equation (8) is exact, as no assumptions or modeling approximations have yet been applied. The exact equation for turbulence kinetic energy, $k = \frac{\{u_i'' u_i''\}}{2}$, is

$$\begin{aligned} \frac{\partial}{\partial x_j} (\langle \rho \rangle \{u_j\} k) &= -\langle \rho \rangle \{u_i'' u_j''\} \frac{\partial \{u_i\}}{\partial x_j} - \left\langle t_{ij}' \frac{\partial u_i''}{\partial x_j} \right\rangle - \langle t_{ij} \rangle \frac{\partial \langle u_i'' \rangle}{\partial x_j} \\ & \quad + \frac{\partial}{\partial x_j} \left(\langle t_{ij} u_i'' \rangle - \langle \rho \rangle \left\{ u_j'' \frac{u_i'' u_i''}{2} \right\} \right) - \frac{\partial \langle p' u_j'' \rangle}{\partial x_j} - \langle u_i'' \rangle \frac{\partial \langle p \rangle}{\partial x_i} + \left\langle p' \frac{\partial u_i''}{\partial x_i} \right\rangle. \end{aligned} \quad (9)$$

Subtracting (9) from (8) leads to the averaged internal energy equation (4). To reach the form (4), the following identity [21] is used:

$$\langle \rho \rangle \{u_j'' h''\} = \langle \rho \rangle \{u_j'' e''\} + \langle p' u_j'' \rangle + \langle p \rangle \langle u_j'' \rangle. \quad (10)$$

RANS models that solve an equation for k apply various assumptions and closures to (9), which can impact the internal energy equation that is effectively satisfied by solutions to the full system of RANS conservation equations. These effects become evident by applying these approximate treatments to (9) and then subtracting the resulting equation from (8). In many two-equation model formulations, the last three terms appearing in (9)—pressure diffusion, pressure work, and turbulent pressure dilatation, respectively—are ignored. Additionally, the dissipation term $\langle t_{ij} \rangle \frac{\partial \langle u_i'' \rangle}{\partial x_j}$ is either ignored or is included in the definition of turbulent dissipation [22]. With these modeling approximations, the resulting averaged internal energy equation is

$$\begin{aligned} & \frac{\partial}{\partial x_j} (\langle \rho \rangle \{u_j\} \{e\}) + \frac{\partial}{\partial x_j} (\langle \rho \rangle \{u_j'' e''\} + \langle p' u_j'' \rangle + \langle p \rangle \langle u_j'' \rangle) \\ &= -\frac{\partial \langle q_j \rangle}{\partial x_j} - \langle p \rangle \frac{\partial \{u_j\}}{\partial x_j} + \langle t_{ij} \rangle \frac{\partial \{u_j\}}{\partial x_j} + \left\langle t_{ij}' \frac{\partial u_i''}{\partial x_j} \right\rangle. \end{aligned} \quad (11)$$

The molecular heat flux, turbulent dissipation, mean pressure dilatation, and mean dissipation terms in (11) all have counterparts in the exact averaged internal energy equation (4). The turbulent pressure-dilatation term is missing because it was neglected in the k equation. Likewise, the term $\langle t_{ij} \rangle \frac{\partial \langle u_i'' \rangle}{\partial x_j}$ is missing because it, too, was neglected in the k equation. Surprisingly, a spurious turbulent energy flux appears in (11), resulting from neglect of the pressure diffusion and pressure work terms. The total turbulent energy flux term in (11) is actually the turbulent enthalpy flux [by (10)], and can be written

$$\frac{\partial}{\partial x_j} (\langle \rho \rangle \{u_j'' e''\} + \langle p' u_j'' \rangle + \langle p \rangle \langle u_j'' \rangle) = \frac{\partial}{\partial x_j} (\langle \rho \rangle \{u_j'' e''\} + \langle p' u_j'' \rangle) + \langle p \rangle \frac{\partial u_j''}{\partial x_j} + \langle u_j'' \rangle \frac{\partial \langle p \rangle}{\partial x_j}. \quad (12)$$

Equation (12) shows that the neglect of the pressure diffusion term leads to its inclusion as a spurious part of the turbulent energy flux. The third term on the right-hand side of (12), when combined with the term $\langle p \rangle \frac{\partial \{u_j\}}{\partial x_j}$ in (11), gives the mean pressure-dilatation term from the exact equation (4). The last term in (12) is an additional spurious contribution due to neglect of the pressure work term. Thus, neglect of the pressure diffusion and pressure work terms have had an undesirable effect

on the effective internal energy balance, with potential implications for how the model represents turbulent transfer of heat.

A common modification applied to turbulence models is to neglect the turbulence kinetic energy in the total energy. The rationale for this approximation is that, for many flows $k \ll \{h\}$, and the turbulence kinetic energy has a negligible effect on the total energy balance. With this approximation, and assuming stationary flow, such that the time derivative term is zero, the total energy equation is

$$\frac{\partial}{\partial x_j} \left[\langle \rho \rangle \{u_j\} \left(\{h\} + \frac{\{u_i\}\{u_i\}}{2} \right) \right] + \frac{\partial}{\partial x_j} [\langle \rho \rangle (\{h''u_j''\} + \{u_i\}\{u_i''u_j''\})] = \frac{\partial}{\partial x_j} (\langle t_{ij} \rangle \{u_i\} - \langle q_j \rangle). \quad (13)$$

Subtracting (7) from (13) and rearranging terms as before leads to the following effective internal energy equation:

$$\begin{aligned} & \frac{\partial}{\partial x_j} (\langle \rho \rangle \{u_j\} \{e\}) + \frac{\partial}{\partial x_j} (\langle \rho \rangle \{u_j''e''\} + \langle p'u_j''\rangle + \langle p \rangle \langle u_j''\rangle) \\ & = -\frac{\partial \langle q_j \rangle}{\partial x_j} - \langle p \rangle \frac{\partial \{u_j\}}{\partial x_j} + \langle t_{ij} \rangle \frac{\partial \{u_j\}}{\partial x_j} - \langle \rho \rangle \{u_i''u_j''\} \frac{\partial \{u_i\}}{\partial x_j}. \end{aligned} \quad (14)$$

The same deficiencies appear in (14) as in (11), namely, the absence of a turbulent pressure-dilatation term and the appearance of spurious contributions to the turbulent energy flux. In addition, the turbulent dissipation is missing from (14); in its place appears a production term (the fourth term on the right-hand side). Van Driest similarly neglected k in his energy analysis for turbulent boundary layers and derived similar production terms in a mean energy equation, which he deemed ‘‘apparent dissipation’’ [23]. In some regions of turbulence, where production is approximately balanced by dissipation, this form of the internal energy equation may be adequate. However, in other regions of the flow, in particular where the magnitude of turbulent dissipation is significant relative to other terms in the energy balance, this formulation could lead to inaccuracies.

We conclude this section by noting that for turbulence models that do not solve an equation for k , the total energy equation typically solved is (13) and the resulting implied internal energy equation will also resemble (14).

III. INTEGRAL EXPRESSIONS FOR WALL HEAT FLUX CONTRIBUTIONS

For convenience, we adopt symbols for some of the terms appearing in the internal energy equations. We denote the mean viscous dissipation per unit volume using either Reynolds- or Favre-averaged velocity, as

$$\Phi^{RA} \equiv \langle t_{ij} \rangle \frac{\partial \langle u_i \rangle}{\partial x_j}, \quad \Phi^{FA} \equiv \langle t_{ij} \rangle \frac{\partial \{u_i\}}{\partial x_j}. \quad (15)$$

This term represents the generation of heat by mean aerodynamic friction. The turbulent dissipation rate per unit volume is the heat generated by the dissipation of mechanical turbulent energy at the smallest scales of the turbulent energy cascade:

$$\phi = \langle \rho \rangle \epsilon \equiv \left\langle t'_{ij} \frac{\partial u'_i}{\partial x_j} \right\rangle = \left\langle t'_{ij} \frac{\partial u''_i}{\partial x_j} \right\rangle. \quad (16)$$

The mean pressure-dilatation terms represent the work done by mean compression or expansion of the flow:

$$\Pi^{RA} \equiv \langle p \rangle \frac{\partial \langle u_i \rangle}{\partial x_i}, \quad \Pi^{FA} \equiv \langle p \rangle \frac{\partial \{u_i\}}{\partial x_i}. \quad (17)$$

The turbulent pressure-dilatation correlation, representing the work done by correlated fluctuations of pressure and dilatation, is

$$\pi \equiv \left\langle p' \frac{\partial u_i'}{\partial x_i} \right\rangle = \left\langle p' \frac{\partial u_i''}{\partial x_i} \right\rangle. \quad (18)$$

Consider an analysis of the compressible turbulent boundary layer on a flat plate, with stream-wise coordinate $x_1 = x$, wall-normal coordinate $x_2 = y$, and span-wise coordinate $x_3 = z$. In particular, we wish to derive an equation relating the wall heat flux to quantities in the boundary layer. We first rewrite (4) as

$$\frac{\partial}{\partial x_j} (\langle \rho \rangle \{e\} \{u_j\}) + \frac{\partial}{\partial x_j} \langle \rho u_j'' e'' \rangle + \frac{\partial \langle q_j \rangle}{\partial x_j} + \Pi^{RA} + \pi - \Phi^{RA} - \phi = I_R. \quad (19)$$

The term I_R represents any imbalance of the stationary terms. For an exact solution, $I_R = 0$, but in practice, I_R may be nonzero due to numerical errors for a RANS or DNS solution, and/or statistical averaging errors for a DNS solution. Following Zhang and Xia [17], we integrate (19) from 0 to y , giving

$$\begin{aligned} & \int_0^y \frac{\partial \langle \rho \rangle \{u\} \{e\}}{\partial x} dy' + \langle \rho \rangle \{v\} \{e\} + \int_0^y \frac{\partial \langle \rho u'' e'' \rangle}{\partial x} dy' + \langle \rho v'' e'' \rangle + \int_0^y \frac{\partial \langle q_x \rangle}{\partial x} dy' \\ & + \langle q_y \rangle - \langle q_w \rangle + \int_0^y \Pi^{RA} dy' + \int_0^y \pi dy' - \int_0^y \Phi^{RA} dy' - \int_0^y \phi dy' = \int_0^y I_R dy', \end{aligned} \quad (20)$$

where we have introduced Cartesian velocity components $(u, v, w) = (u_x, u_y, u_z)$. Equation (20) represents an energy balance over a one-dimensional ‘‘volume,’’ includes the mean wall heat flux $\langle q_w \rangle = \langle q_y|_{y=0} \rangle$, and is valid for any location y . Integrating (20) from 0 to a height, h , above the wall, and applying integration by parts to some terms, gives an expression for the wall heat flux in terms of integrals of the various terms:

$$\begin{aligned} \langle q_w \rangle = & \frac{1}{h} \left[\int_0^h (h-y) \frac{\partial}{\partial x} (\langle \rho \rangle \{u\} \{e\}) dy + \int_0^h \langle \rho \rangle \{v\} \{e\} dy + \int_0^h (h-y) \frac{\partial}{\partial x} (\langle \rho u'' e'' \rangle) dy \right. \\ & + \int_0^h \langle \rho v'' e'' \rangle dy + \int_0^h (h-y) \frac{\partial \langle q_x \rangle}{\partial x} dy + \int_0^h \langle q_y \rangle dy + \int_0^h (h-y) \Pi^{RA} dy \\ & \left. + \int_0^h (h-y) \pi dy + \int_0^h (y-h) \Phi^{RA} dy + \int_0^h (y-h) \phi dy + \int_0^h (y-h) I_R dy \right]. \end{aligned} \quad (21)$$

Equation (21) gives the integrated contribution of each physical process to the wall heat flux. The flux terms, such as molecular heat flux, are simply integrals of the flux, while the ‘‘source term’’ contributions, such as the viscous dissipation, have integrands that are weighted by the distance from the upper integration limit. The integral terms on the right-hand side of (21), in order of appearance, are subsequently referred to as mean stream-wise convection (I_C), mean wall-normal convection (I_C), stream-wise turbulent heat transfer (I_T), wall-normal turbulent heat transfer (I_T), stream-wise molecular heat transfer (I_{q_x}), wall-normal molecular heat transfer (I_{q_y}), mean pressure dilatation (I_Π), turbulent pressure dilatation (I_τ), mean dissipation (I_ϕ), and turbulent dissipation (I_ϕ).

As discussed in Sec. I, various integral expressions relating wall quantities to interior terms have been derived in the literature for wall-bounded turbulent flow. Such expressions are not unique; for example, as discussed in Wenzel *et al.* [18], an infinite sequence of integral expressions for the wall shear stress or wall heat flux can be generated by applying n -fold integration, with any choice of positive integer n . Here, we chose twofold integration, since a single integration [giving (20)] does not result in integrated contributions by the flux terms over the region of interest. A double integration, given by (21) is the simplest expression that results in terms that describe an average contribution of each term over the integration volume. By choosing to integrate the internal energy

equation and by maintaining each term in its original form from the governing differential equation, each term represents a distinct physical process. However, integration over a region of space, as well as the presence of a weighting by $(h - y)$ in some of the terms, does complicate a physical interpretation of the decomposition. We emphasize that we are primarily interested in studying the effects of various closure modeling strategies on predicted wall heat flux and, in the present form, terms that require modeling are preserved and easily identified.

Other energy equations can be integrated to give an expression for wall heat flux, such as the total enthalpy equation, and this is useful for certain purposes such as evaluation of the strong Reynolds analogy [18]. However, total enthalpy or total energy equations such as (6) are conservation laws that describe a flux balance of the sum of internal and kinetic energy over a volume, wherein terms that describe energy exchanges among the components of the total energy, such as generation of heat by mean and turbulent dissipation, are masked. The internal energy equation used here serves as the elemental equation for the study of heat transfer within the flow, containing explicit terms for the generation and transfer of internal energy and the resulting loss (or gain) of heat through the wall flux. In the modeling context, this choice of internal energy over enthalpy also helps eliminate ambiguous terms arising in RANS models, such as moments with the unsteady pressure, and for high-speed shear flows with thermal nonequilibrium, the internal energy has proven to be the natural variable when characterizing the internal state of molecules. A similar choice of internal energy was made by Bowersox and coworkers when deriving the algebraic energy flux model [24,25].

We note that the upper integration limit in (21), which we will choose later as $h = \delta$, where δ is the boundary layer thickness, is arbitrary. The integral terms do not all reach an asymptotic state with increasing wall distance by $h = \delta$. Note also that some of the terms asymptote to zero as $h \rightarrow \infty$, while other terms asymptote to a nonzero constant for $h \rightarrow \infty$. Thus, the expression is not useful for decomposition of the wall heat flux into a discrete set of physical processes over the full domain ($h \rightarrow \infty$), as was accomplished in Renard and Deck [26] for boundary layer wall shear stress. However, the utility of the expression is maintained even though it depends on the choice of integration volume. The important factor in the analysis is choosing a physically meaningful integration volume. In our case, setting the integration limit to be the boundary layer edge allows us to assess *the net contribution of each term in the averaged internal energy equation to the wall heat flux, averaged over the turbulence-containing region*. Furthermore, we confirmed that the qualitative behavior of the relative contributions does not change as the upper integration bound is extended beyond the boundary layer thickness, as shown in Appendix A.

IV. RANS MODELS

We consider several commonly used RANS models for external aerodynamics applications: the algebraic Baldwin-Lomax model (BL) [27], the one-equation Spalart-Allmaras model (SA) [28,29], and the two-equation Menter shear stress transport (SST) model (SST-V2003) [30]. Two modifications to the SST-V2003 model are also considered in this paper: neglect of the turbulence kinetic energy in the total energy equation and application of the Zeman compressibility correction. Both of these modifications are described below. The SST and SA model solutions were obtained using the Sandia Parallel Aerodynamics and Reentry Code (SPARC) [31], while the BL model solutions were obtained using the NASA CFL3D code [32].

We first describe commonly shared features of the three models. All three models are applied to the Favre-averaged Navier-Stokes equations. In addition to the averaged total energy equation (6), the following averaged mass and momentum equations are solved:

$$\frac{\partial}{\partial x_j} (\langle \rho \rangle \{u_j\}) = 0, \quad (22)$$

$$\frac{\partial}{\partial x_j} (\langle \rho \rangle \{u_i\} \{u_j\}) + \frac{\partial \langle p \rangle}{\partial x_i} = \frac{\partial}{\partial x_j} (\langle t_{ij} \rangle - \langle \rho \rangle \{u_i'' u_j''\}). \quad (23)$$

The models compute the Reynolds stress tensor according to the following Boussinesq relationship:

$$\tau_{ij} = -\langle \rho \rangle \{u_i'' u_j''\} = 2\mu_T \left(\{S_{ij}\} - \frac{1}{3} \frac{\partial \{u_k\}}{\partial x_k} \delta_{ij} \right) - \frac{2}{3} r_m \langle \rho \rangle k \delta_{ij}, \quad (24)$$

where $r_m = 1$ for the SST-V2003 model and $r_m = 0$ for the BL and SA models. The models differ in their calculation of the eddy viscosity, μ_T . Each model uses a gradient transport closure for the turbulent heat flux:

$$\langle \rho \rangle \{u_j'' h''\} = -\frac{\mu_T C_p}{\text{Pr}_T} \frac{\partial \{T\}}{\partial x_j}. \quad (25)$$

The turbulent Prandtl number, Pr_T , is set to a constant value of 0.9. The mean viscous stress tensor is evaluated according to

$$\langle t_{ij} \rangle \approx 2\mu(\{T\}) \{S_{ij}\} - \frac{2}{3} \mu(\{T\}) \frac{\partial \{u_k\}}{\partial x_k} \delta_{ij}, \quad (26)$$

while the molecular heat flux is evaluated as

$$\langle q_j \rangle \approx -\frac{\mu(\{T\}) C_p}{\text{Pr}} \frac{\partial \{T\}}{\partial x_j}, \quad (27)$$

with constant Prandtl number, Pr , equal to 0.71. Note that (26) and (27) are approximate, since Favre-averaged velocity and temperature have been substituted for their Reynolds-averaged counterparts, and correlations between transport coefficient fluctuations and velocity/temperature gradient fluctuations have been ignored [33]. The former approximation is a result of using Favre-averaged variables in the nonconvective terms, while the latter is typically considered valid but may require further scrutiny for hypersonic flows.

A. SST-V2003 model

The SST-V2003 model is a two-equation model, solving two additional transport equations for the Favre-averaged turbulence kinetic energy and the specific dissipation rate:

$$\frac{\partial}{\partial x_j} (\langle \rho \rangle \{u_j\} k) = P - \beta^* \langle \rho \rangle \omega k + \frac{\partial}{\partial x_j} \left[(\mu(\{T\}) + \sigma_k \mu_T) \frac{\partial k}{\partial x_j} \right], \quad (28)$$

$$\begin{aligned} \frac{\partial}{\partial x_j} (\langle \rho \rangle \{u_j\} \omega) &= \frac{\gamma \langle \rho \rangle}{\mu_T} P - \beta \langle \rho \rangle \omega^2 + \frac{\partial}{\partial x_j} \left[(\mu(\{T\}) + \sigma_\omega \mu_T) \frac{\partial \omega}{\partial x_j} \right] \\ &+ 2(1 - F_1) \frac{\langle \rho \rangle \sigma_{\omega 2}}{\omega} \frac{\partial k}{\partial x_j} \frac{\partial \omega}{\partial x_j}. \end{aligned} \quad (29)$$

The turbulence kinetic energy production is approximated as

$$P = \mu_T \Omega^2 - \frac{2}{3} \langle \rho \rangle k \delta_{ij} \frac{\partial \{u_i\}}{\partial x_j}, \quad (30)$$

with Ω equal to the mean vorticity magnitude. Usage of the vorticity magnitude in the production term is the reason for the letter “V” appearing in the moniker “SST-V2003.” A production limiter is used such that P is replaced by $\min(P, 10\beta^* \langle \rho \rangle \omega k)$ in both (28) and (29). The molecular diffusion and turbulent transport terms in (9) have been modeled as

$$\langle t_{ij} u_i'' \rangle - \langle \rho \rangle \left\{ u_j'' \frac{u_i'' u_i''}{2} \right\} = (\mu(\{T\}) + \sigma_k \mu_T) \frac{\partial k}{\partial x_j}. \quad (31)$$

These terms are modeled in the same way in the total energy equation (6). The eddy viscosity is calculated from

$$\mu_T = \frac{\langle \rho \rangle a_1 k}{\max(a_1 \omega, SF_2)}, \quad (32)$$

where S is the strain invariant $\sqrt{2S_{ij}S_{ij}}$. Model constants and blending functions for the SST-V2003 model are given in Appendix B.

B. SST-V2003 with Zeman compressibility correction

RANS models have sometimes been modified with compressibility corrections based on modeling of dilatational dissipation. Rumsey [10] found that the correction by Zeman for boundary layer flows [34] performed better for cold-wall hypersonic turbulent boundary layers compared with other corrections designed for free shear layers. The Zeman compressibility correction modifies the constants in the k and ω destruction terms in (28) and (29) as follows:

$$\begin{aligned} \beta_c^* &= \beta^*[1 + \xi^*F(M_T)], & \beta_c &= \beta - \beta^*\xi^*F(M_T), \\ F(M_T) &= \left[1 - \exp\left(-\left(\frac{M_T - M_{T0}}{\Lambda}\right)^2\right) \right] \mathcal{H}(M_T - M_{T0}). \end{aligned} \quad (33)$$

Here, $M_T = \sqrt{2k}/c$ is the turbulence Mach number, with $c = \sqrt{\gamma_g R \{T\}}$ the local speed of sound (with gas constant R and ratio of specific heats γ_g), and with $\xi^* = 0.75$, $M_{T0} = 0.2$, and $\Lambda = 0.66$. $\mathcal{H}(\cdot)$ is the Heaviside function.

C. SST-V2003-nok model

The SST-V2003-nok model is identical to the SST-V2003 model except that the turbulence kinetic energy is neglected in the definition of total energy, and the total energy equation that is solved is Eq. (13).

D. SA model

The SA model involves one additional transport equation. We used the SA-neg-noft2 model [29]. This form of the model involves a change when the working variable becomes negative; otherwise, its behavior is expected to be very close to the standard model. The ‘‘noft2’’ designation means that the trip term is ignored by setting $f_{t2} = 0$ in the standard form of the model; this is sometimes referred to as the ‘‘fully turbulent’’ form of the SA model. The equation for the working variable is

$$\begin{aligned} \frac{\partial}{\partial x_j} (\langle \rho \rangle \{u_j\} \tilde{v}) &= \langle \rho \rangle c_{b1} \tilde{S} \tilde{v} - \langle \rho \rangle c_{w1} f_w \left(\frac{\tilde{v}}{d}\right)^2 + \frac{1}{\sigma} \left[\frac{\partial}{\partial x_j} \left((\mu(\{T\}) + \langle \rho \rangle \tilde{v}) \frac{\partial \tilde{v}}{\partial x_j} \right) + \langle \rho \rangle c_{b2} \frac{\partial \tilde{v}}{\partial x_i} \frac{\partial \tilde{v}}{\partial x_i} \right] \\ &\quad - \frac{1}{\sigma} \left(\frac{\mu(\{T\})}{\langle \rho \rangle} + \tilde{v} \right) \frac{\partial \langle \rho \rangle}{\partial x_i} \frac{\partial \tilde{v}}{\partial x_i}, \end{aligned} \quad (34)$$

where

$$\tilde{S} = \Omega + \frac{\tilde{v}}{\kappa^2 d^2} f_{v2}, \quad \chi = \frac{\langle \rho \rangle \tilde{v}}{\mu(\{T\})}, \quad f_{v2} = 1 - \frac{\chi}{1 + \chi f_{v1}}, \quad f_{v1} = \frac{\chi^3}{\chi^3 + c_{v1}^3}. \quad (35)$$

The eddy viscosity is calculated from

$$\mu_T = \langle \rho \rangle \tilde{v} f_{v1}. \quad (36)$$

Modeling constants and other functions for the SA model not defined above (including f_w) are given in Appendix B. Turbulence kinetic energy does not appear explicitly in the SA model, so that the form of the total energy equation is (13).

E. BL model

The Baldwin-Lomax model is an algebraic model; that is, the eddy viscosity is specified as an algebraic function of the local mean flow-field state. The eddy viscosity is computed from a two-layer model, where

$$\mu_T = \begin{cases} \mu_{T_{\text{inner}}}, & y \leq y_{\text{crossover}} \\ \mu_{T_{\text{outer}}}, & y > y_{\text{crossover}} \end{cases}. \quad (37)$$

The boundary between the two layers, $y_{\text{crossover}}$, is the value of the wall-normal coordinate y where $\mu_{T_{\text{inner}}}$ first exceeds $\mu_{T_{\text{outer}}}$. The inner eddy viscosity is

$$\mu_{T_{\text{inner}}} = \langle \rho \rangle l_m^2 |\Omega|, \quad (38)$$

where

$$l_m = k_l y (1 - e^{-\frac{y^*}{A^+}}), \quad y^* = \frac{\sqrt{\langle \rho \rangle \tau_w}}{\mu(\{T\})} y, \quad (39)$$

$$|\Omega| = \sqrt{2\Omega_{ij}\Omega_{ij}}, \quad \Omega_{ij} = \frac{1}{2} \left(\frac{\partial \{u_i\}}{\partial x_j} - \frac{\partial \{u_j\}}{\partial x_i} \right). \quad (40)$$

The quantity y^* , using local scaling, has been used rather than the original y^+ ; this has been found to improve calculations of compressible boundary layers with appreciable mean temperature gradients [9]. The outer eddy viscosity is

$$\mu_{T_{\text{outer}}} = \langle \rho \rangle K C_{CP} F_{\text{WAKE}} F_{\text{KLEB}}(y). \quad (41)$$

The model constants and functions required in (39) and (41) are given in Appendix B.

V. DNS SOLUTIONS

The DNS simulates an experiment for a nominally Mach 11.1 turbulent boundary layer on a cold-wall flat plate with $T_w/T_r = 0.2$ and Reynolds number up to $\text{Re}_\tau = 1193$ that was performed at the Calspan–University of Buffalo Research Center (CUBRC) [4,35]. The CUBRC configuration has previously been used for verification and validation of RANS models and is denoted as CUBRC run 7. In the DNS, the high-speed turbulent boundary layer is simulated by solving the conservative-variables formulation of the full three-dimensional compressible Navier-Stokes equations. The working fluid is assumed to be a perfect gas, and the usual constitutive relations for a Newtonian fluid are used. Sutherland’s law is used to compute the temperature-dependent viscosity. A seventh-order weighted essentially nonoscillatory scheme (WENO) is used for the spatial discretization of inviscid fluxes for the DNS case. To reduce the numerical dissipation, the current scheme is optimized by means of limiters [36,37], compared to the original WENO introduced by Ref. [38]. The viscous fluxes are discretized using a fourth-order central difference scheme, and the time marching is a third-order low-storage Runge-Kutta scheme [39]. The validity of the numerical methodology for simulating supersonic and hypersonic turbulent boundary layers has been shown in multiple previous studies, including [19,37,40–44], among others. The inflow boundary condition of the DNS is prescribed by means of a recycling-rescaling method [42], and the simulation covered a long streamwise domain (greater than $300\delta_i$, with δ_i the inflow boundary-layer thickness) to guarantee the settlement of turbulence statistics into a fully developed equilibrium state of the turbulent boundary layer. The details of the DNS methodology, including numerical methods and boundary conditions, have been documented in a previous paper [19].

The DNS database has been used to compute contributions of each integral term in (21) with $h = \delta$, and these are tabulated for two different values of Re_τ in Table I. A positive sign on the contribution to the wall heat flux coefficient $B_q = q_w / (\rho_w C_p T_w u_\tau)$, with C_p being the specific heat at constant pressure and u_τ being the friction velocity, indicates net transfer of heat into the fluid domain (away from the wall), while a negative sign indicates a net transfer out of the domain (toward

TABLE I. Average contribution, across the boundary layer, of terms in the internal energy equation to wall heat flux (DNS results).

Mechanism	B_q		Contribution to wall heat flux (%)		
	$Re_\tau = 774$	$Re_\tau = 1172$	$Re_\tau = 774$	$Re_\tau = 1172$	Mach 3 channel, $Re_\tau = 456$ [17]
Wall-normal molecular heat transfer (I_{q_y})	8.49×10^{-4}	5.69×10^{-4}	0.18	0.13	5.34
Stream-wise molecular heat transfer (I_{q_x})	1.52×10^{-4}	1.31×10^{-4}	0.03	0.03	
Wall-normal turbulent heat transfer (I_{T_y})	6.02×10^{-2}	5.81×10^{-2}	12.61	13.23	4.39
Stream-wise turbulent heat transfer (I_{T_x})	9.48×10^{-4}	-4.42×10^{-4}	0.20	0.10	
Wall-normal mean convection (I_{C_y})	5.52×10^{-2}	4.93×10^{-2}	11.56	11.23	
Stream-wise mean convection (I_{C_x})	-2.33×10^{-2}	-2.25×10^{-2}	4.88	5.12	
Mean pressure dilatation (I_Π)	4.01×10^{-2}	3.73×10^{-2}	8.40	8.48	
Turbulent pressure dilatation (I_π)	-2.88×10^{-3}	-1.84×10^{-3}	0.60	0.42	1.46
Turbulent dissipation (I_ϕ)	-1.22×10^{-1}	-1.23×10^{-1}	25.55	27.95	88.4*
Mean dissipation (I_Φ)	-1.65×10^{-1}	-1.43×10^{-1}	34.51	32.54	*($I_\phi + I_\Phi$)
Residual	-7.10×10^{-3}	-3.38×10^{-3}	1.49	0.77	
Total	-0.1627	-0.1484	100	100	100
Direct wall heat flux	-0.1628	-0.1484			

the wall). A percentage is calculated for each net contribution using the ratio of the absolute value of the contribution to the sum of the absolute values of all contributions. The relative contributions differ significantly from those computed for compressible channel flow at Mach 1.5 and Mach 3.0 [17]. For comparison purposes, the fractional contributions for the Mach 3.0 channel DNS at $Re_\tau = 456$ from Ref. [17] are included in the right-most column of Table I. The wall-normal turbulent heat flux contribution is larger than for channel flow, and, unlike for the channel flow, opposes the dissipation contributions. The mean convection contributions and mean pressure dilatation are non-negligible, while for channel flow they are identically zero. The turbulent pressure dilatation has a somewhat smaller effect (less than 1%) for the present flow than for the channel results at lower Mach number, consistent with the trend showed in Ref. [17] of decreasing relative importance of this term with increasing Mach number. The mean and turbulent dissipation contributions are the largest, while both components of the molecular heat flux contribution are small. Some of the contributions to B_q change significantly between the two Reynolds numbers considered; however, changes in the percentage contribution are modest for all the terms. The residual contribution is less than 2% for both Reynolds numbers, and the B_q calculated from the integral balance agrees with the direct calculation of the mean molecular wall heat flux using the DNS solution to three digits.

Figure 2 shows the integral contributions to wall heat flux as a function of the integration limit, h , up to the height of the boundary layer. Components with negligible net contribution for $h = \delta$ are omitted from the plots, except for the wall-normal molecular heating contribution (I_{q_y}). Note that very close to the wall, the wall-normal molecular heat transfer contribution (I_{q_y}) is dominant and becomes the sole contribution at the wall, $y = 0$ (l'Hospital's rule gives $\lim_{h \rightarrow 0} \frac{1}{h} \int_0^h \langle q_y \rangle dy = \langle q_y(0) \rangle$); its net effect diminishes rapidly as integration height increases, however. The net contribution of the mean dissipation over the boundary layer approximately equals the wall heat flux itself for both Reynolds numbers, with the net effect of the sum of all other contributions close to zero. Wall-normal turbulent heat transfer (I_{T_y}), mean pressure dilatation (I_Π), turbulent dissipation (I_ϕ), and mean dissipation (I_Φ) dominate the contributions for $y/\delta \lesssim 0.3$, with the two mean convection components (I_{C_x} , I_{C_y}) becoming significant at larger distances from the wall. The effect of increasing the upper integration bound beyond the boundary layer thickness is discussed in Appendix A.

For later comparison to RANS model behavior, it is useful to present the wall-normal turbulent heat flux and mean pressure-dilatation terms as they appear in RANS models which use Favre-

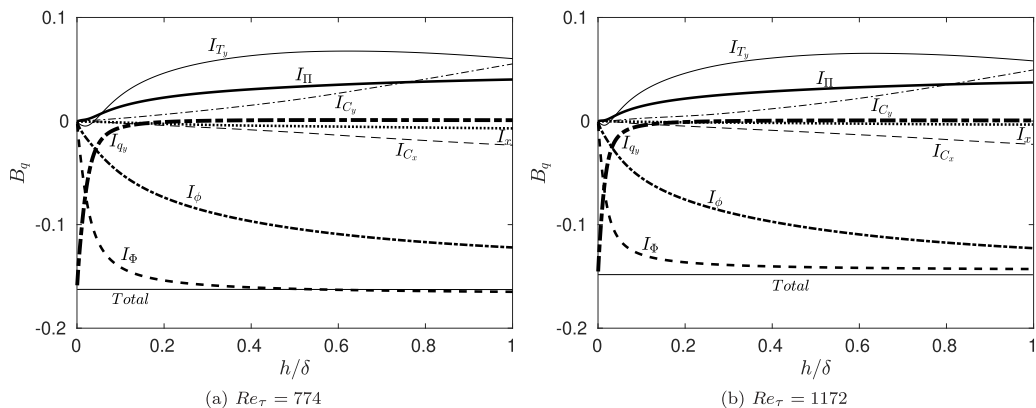


FIG. 2. Integrated contributions of terms in the internal energy equation to the nondimensional wall heat flux from the DNS. The physical mechanism acronyms are defined in Table I.

averaged variables. Figure 3 shows these profiles using the DNS data, where the mean pressure dilatation is evaluated using the Favre-averaged dilatation $\frac{\partial \langle u_j' \rangle}{\partial x_j}$, and the contribution $\langle p \rangle \frac{\partial \langle u_j' \rangle}{\partial x_j}$ is included in the turbulent heat flux. The turbulent heat flux contribution (I_{T_y}) is also included in the figure for comparison. At both Reynolds numbers, the contribution $I_{T_y} \equiv I_{T_y} + \langle p \rangle \frac{\partial \langle u_j' \rangle}{\partial x_j}$ is about 40% larger than the contribution from I_{T_y} alone. The mean pressure-dilatation contribution calculated from the Favre-averaged velocity, $I_{\Pi} \equiv \langle p \rangle \frac{\partial \langle u_j \rangle}{\partial x_j}$ is about 60% lower than that calculated from the Reynolds-averaged velocity (cf. Fig. 2).

Recall that in Sec. II we showed how neglect of the pressure diffusion and pressure work terms in the RANS turbulence kinetic energy equation led to their appearance as spurious terms in the internal energy balance; see Eq. (11). We assessed the potential effect of these spurious contributions by calculating their integrated effects over the boundary layer from the DNS solutions and found that these terms would make negligible contributions to the wall flux (less than 0.2% change to the magnitude of $\langle q_w \rangle$), thus validating their neglect for the present flow. We note, however, that pressure diffusion can take on non-negligible magnitudes in other high-speed flows, such as in shock wave-boundary layer interaction [45]. The missing contribution to the mean dissipation involving

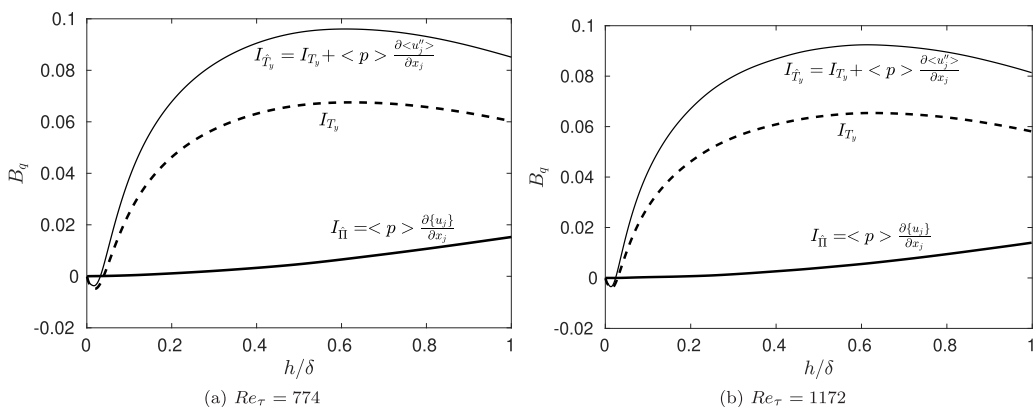


FIG. 3. Integrated contributions of heat flux and mean pressure dilatation terms to the wall heat flux from DNS. The terms are modified to match the form seen in RANS solutions using Favre-averaged variables.

the turbulent mass flux that arises from usage of Favre-averaged velocity in RANS, $\langle t_{ij} \rangle \frac{\partial \langle u'_j \rangle}{\partial x_j}$, was found to modify the wall heat flux by only about 1%.

For high Mach number, cold-wall boundary layers the dissipation of turbulence kinetic energy can have non-negligible components due to compressibility effects. The dissipation in a compressible medium can be decomposed into three components [46],

$$\phi = \phi_1 + \phi_2 + \phi_3, \quad (42)$$

where

$$\phi_1 = \langle \mu \rangle \left\langle \frac{\partial u'_i}{\partial x_k} \left(\frac{\partial u'_i}{\partial x_k} + \frac{\partial u'_k}{\partial x_i} \right) \right\rangle - \frac{2}{3} \langle \mu \rangle \left\langle \frac{\partial u'_i}{\partial x_k} \frac{\partial u'_i}{\partial x_l} \right\rangle \delta_{ik}, \quad (43)$$

$$\phi_2 = \left\langle \mu' \frac{\partial u'_i}{\partial x_k} \left(\frac{\partial u'_i}{\partial x_k} + \frac{\partial u'_k}{\partial x_i} \right) \right\rangle - \frac{2}{3} \left\langle \mu' \frac{\partial u'_i}{\partial x_k} \frac{\partial u'_i}{\partial x_l} \right\rangle \delta_{ik}, \quad (44)$$

$$\phi_3 = \left\langle \mu' \frac{\partial u'_i}{\partial x_k} \right\rangle \left(\frac{\partial \langle u_i \rangle}{\partial x_k} + \frac{\partial \langle u_k \rangle}{\partial x_i} \right) - \frac{2}{3} \left\langle \mu' \frac{\partial u'_i}{\partial x_k} \right\rangle \frac{\partial \langle u_l \rangle}{\partial x_l} \delta_{ik}. \quad (45)$$

The component ϕ_1 can be further divided into solenoidal, dilatational, and inhomogeneous contributions,

$$\phi_1 = \phi_s + \phi_d + \phi_I, \quad (46)$$

$$\phi_s = 2 \langle \mu \rangle \langle \omega'_{ij} \omega'_{ij} \rangle; \text{ with } \omega'_{ij} = \left(\frac{\partial u'_i}{\partial x_j} - \frac{\partial u'_j}{\partial x_i} \right) / 2, \quad (47)$$

$$\phi_d = \frac{4}{3} \langle \mu \rangle \left\langle \frac{\partial u'_i}{\partial x_l} \frac{\partial u'_k}{\partial x_k} \right\rangle, \quad (48)$$

$$\phi_I = 2 \langle \mu \rangle \left(\frac{\partial^2 \langle u'_i u'_j \rangle}{\partial x_i \partial x_j} - 2 \frac{\partial}{\partial x_i} \left\langle u'_i \frac{\partial u'_j}{\partial x_j} \right\rangle \right). \quad (49)$$

A typical RANS model that includes a transport equation for $\phi = \langle \rho \rangle \epsilon$ formally models the solenoidal component of dissipation, while the other components are neglected, with the possible exception of the dilatational component, which is sometimes explicitly modeled. The contribution of the turbulent dissipation to the wall heat flux can be separated into distinct contributions from each of the components in (42)–(49). Figure 4(a) shows that the nonsolenoidal components of dissipation contribute a small but noticeable amount to the wall heat flux, comprising about 6% of the total turbulent dissipation contribution. Figure 4(b) shows the contributions to the wall heat flux of the individual nonsolenoidal components. Despite ϕ_3 reaching the largest peak value of these components, consistent with previous DNS results for compressible channel flow [46], it is ϕ_2 that has the largest average contribution to the wall heat flux over the boundary layer. The direct influence of dilatational dissipation on wall heat flux is small, and the effect of the inhomogeneous component is negligible.

VI. RANS MODEL ASSESSMENT FOR WALL HEAT FLUX PREDICTIONS

RANS solutions for the nominally Mach 11 boundary layer were computed on three grids, labeled coarse, medium, and fine. The number of grid cells in the streamwise direction, N_x , doubled for each grid refinement, varying from 362 to 1442. The number of grid cells in the wall-normal direction was $N_y = 140$ for the coarse grid, $N_y = 200$ for the medium grid, and $N_y = 336$ for the fine grid. The grids were extruded in the wall-normal direction, with initial wall-normal grid spacing varying from $\Delta y_1 = 3 \times 10^{-6}$ m on the coarse grid to $\Delta y_1 = 7.5 \times 10^{-7}$ m on the fine

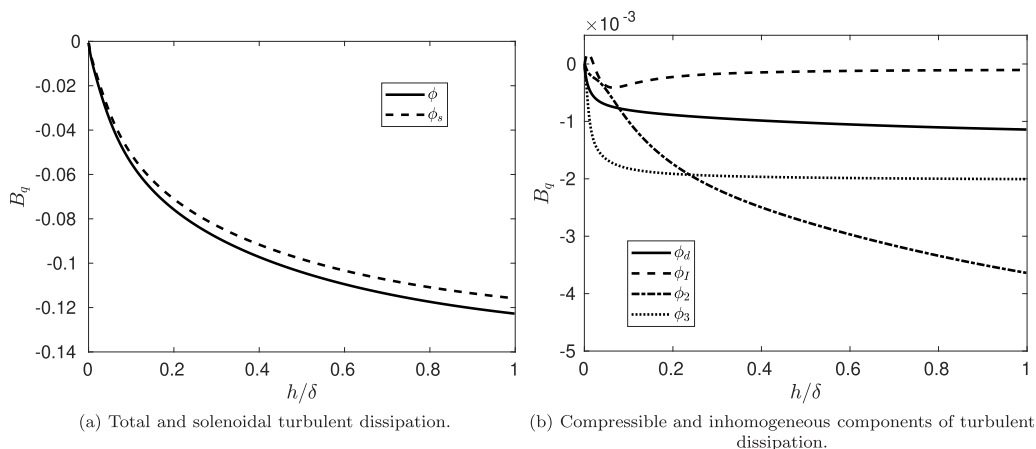


FIG. 4. Integrated contributions of the various components of turbulent dissipation to the wall heat flux from DNS, $Re_\tau = 1172$.

grid; cell growth rate was limited to 1.07 in the wall-normal direction for each grid. Solution accuracy was assessed by examining the grid convergence of the wall heat flux at the stream-wise location corresponding to the DNS friction Reynolds numbers of $Re_\tau = 774$ and $Re_\tau = 1172$, as calculated on the fine grid. For all variants of the SST model, the wall heat flux varied by less than 0.6% between the medium and fine mesh for $Re_\tau = 774$, and by less than 0.5% for $Re_\tau = 1172$. Calculated grid convergence index (GCI) [47] for the SST models was less than 1.1% for both locations. For the SA model, the wall heat flux varied by 0.02% between the medium and fine mesh for $Re_\tau = 774$ and by less than 0.01% for $Re_\tau = 1172$. GCI could not be estimated for the SA solutions due to nonmonotonic convergence behavior with grid refinement. For the BL solutions, the wall heat flux for $Re_\tau = 774$ varied between the medium and fine mesh by 0.3% and by 0.2% for $Re_\tau = 1172$, with GCI less than 1.1% at both locations. Solutions for all models were relaxed to steady state, with nonlinear residual values decreasing at least 11 orders of magnitude for SA solutions, 13 orders of magnitude for SST solutions, and nine orders of magnitude for Baldwin-Lomax solutions. Iterative convergence errors were determined to be negligible.

Mean velocity and temperature profiles for the RANS solutions on the fine grid are compared to DNS in Fig. 5. The mean velocity used for the comparisons is the transformed velocity from the total-stress transformation for compressible boundary layers [48]. This transformed velocity is defined by $U_{\text{tot}}^+(y^*) = \int S_{\text{tot}}^+ dy^*$, where $S_{\text{tot}}^+ = \frac{S_{\text{eq}}^+}{1 + S_{\text{eq}}^+ - S_{\text{TL}}^+}$, with $S_{\text{eq}}^+ = \frac{\mu_w}{\mu} \frac{\partial U^+}{\partial y^*}$ and $S_{\text{TL}}^+ = \frac{\mu}{\mu_w} \frac{\partial U^+}{\partial y^*}$, and the semilocal coordinate is $y^* = \frac{y\sqrt{\rho\tau_w}}{\mu}$. Variables with a $+$ superscript are nondimensionalized by the usual inner viscous scales. The total stress transformation has been shown to successfully collapse the inner layers of various compressible boundary layer velocity profiles to the canonical incompressible form. The present DNS profile is also successfully transformed, albeit with some ambiguity remaining in whether the transformed profile truly demonstrates the presence of a logarithmic layer [19]. The BL model agrees best with the DNS for prediction of mean velocity profile, while the other models deviate significantly from the DNS. The mean temperature profiles demonstrate similar levels of deviation from the DNS. The SA model underpredicts the mean temperature over much of the profile, the BL model overpredicts mean temperature, and the SST model variants give the best overall agreement with the DNS for mean temperature.

The integral contributions to heat flux for the RANS solutions were computed by postprocessing the cell-centered solution fields generated by the CFD codes. Gradients were computed using second-order finite difference formulas, while integrations were computed by taking the cell-center solution value as piece-wise constant, consistent with the cell-centered finite volume scheme used

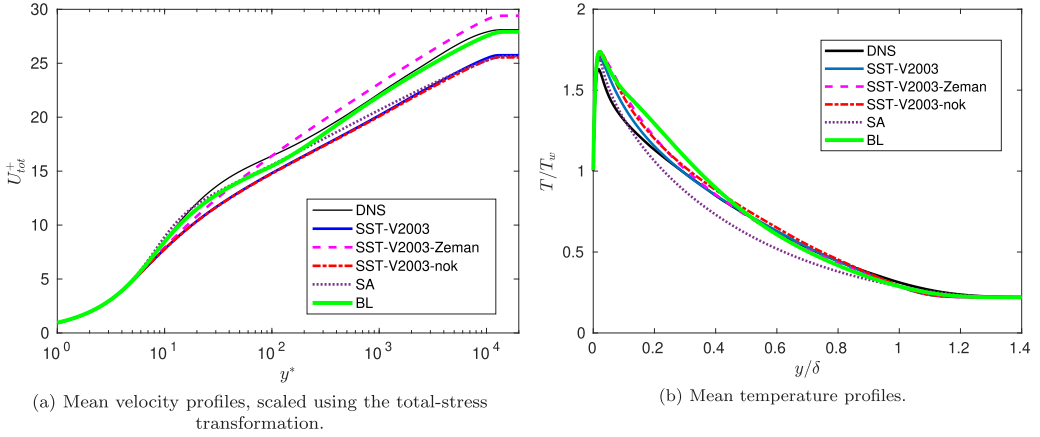


FIG. 5. Comparison of RANS model solutions for mean velocity and temperature to DNS.

in the CFD code. The magnitude of the postprocessing numerical errors is examined by calculating the integral contributions for the various terms on the several grid levels and assessing convergence. Figure 6 shows the most important integral contributions as calculated on the three grids for the SST-V2003 model at $Re_\tau = 774$. At $h = \delta$, the relative errors between the medium and fine grid solutions are less than 2% for the I_Φ , I_ϕ , I_{T_y} , and I_{C_x} contributions. The relative error for the I_{C_y} contribution is 4.6%, while the relative error for the $I_{\hat{\Pi}}$ contribution is largest at 26.7%. However, the absolute error in the contribution to B_q for both of these latter two terms is less than 0.004, which is only about 2% of the net wall heat flux value. The residual B_q contribution (not shown in the figure) decreased from -0.062 on the coarse mesh to -0.0048 on the fine mesh. All subsequent solutions presented in this paper were obtained on the fine mesh.

Figures 7 through 9 show contributions of the turbulent heat flux, mean dissipation, and turbulent dissipation to wall heat flux as a function of integration height for the RANS solutions, for $Re_\tau = 1172$. The mean pressure dilatation and mean convection contributions from the RANS solutions for all the models agree well with the DNS, and are not plotted. Figure 7 shows that

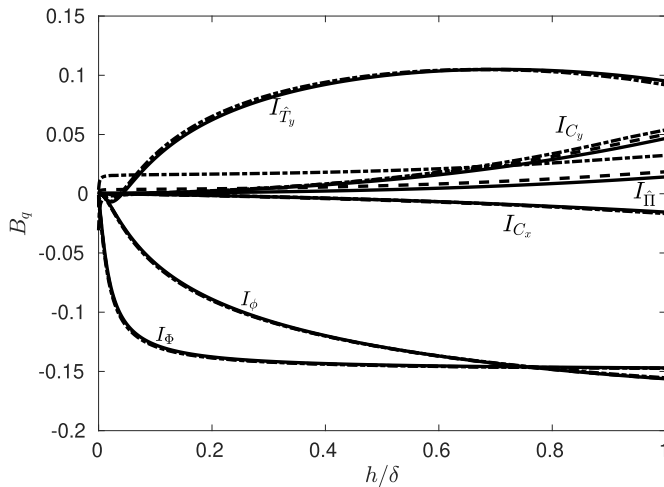


FIG. 6. Grid sensitivity of integral wall heat flux contributions for the SST-V2003 model, $Re_\tau = 774$. — fine grid; --- medium grid; ···· coarse grid. The physical mechanism acronyms are defined in Table I.

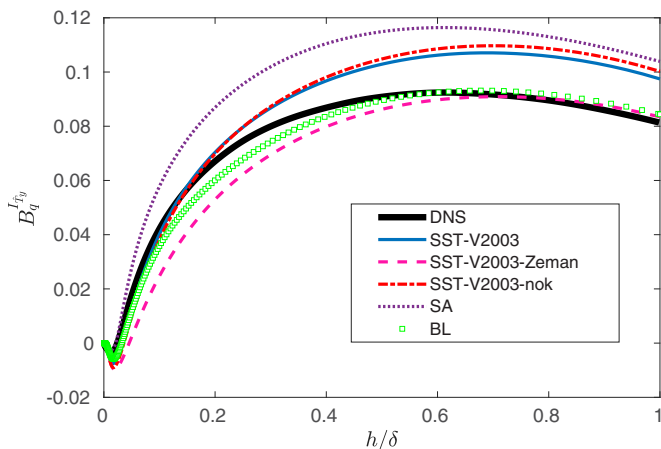


FIG. 7. Integrated contributions of the wall-normal turbulent heat flux term (I_T) in the internal energy equation to the nondimensional wall heat flux, $\text{Re}_\tau = 1172$.

the wall-normal turbulent heat flux contribution from the RANS solutions is larger than that from the DNS for the SST-V2003, SST-V2003-nok, and SA models. For these models at $h = \delta$, it is approximately 20–25% larger than the DNS. The error in the turbulent heat flux contribution is much smaller for the SST-V2003-Zeman and BL models. The contributions from the mean dissipation (Fig. 8) and turbulent (or apparent) dissipation (Fig. 9) integrals are different for each model. Neglecting the turbulent kinetic energy in the SST-V2003-nok model had a minimal effect on all the contributions; in this case, the apparent dissipation provided a similar contribution as the turbulent dissipation. However, the compressibility correction in the SST-V2003-Zeman model had an effect on all three contributions. The magnitude of the negative contribution from mean dissipation is markedly decreased, with a smaller decrease in the magnitude of the turbulent dissipation contribution. These decreases in the magnitude of the dissipation contributions are partially offset by the decrease in the positive turbulent heat flux contribution noted earlier. The net effect of these changes is that the compressibility correction gives a smaller negative wall heat

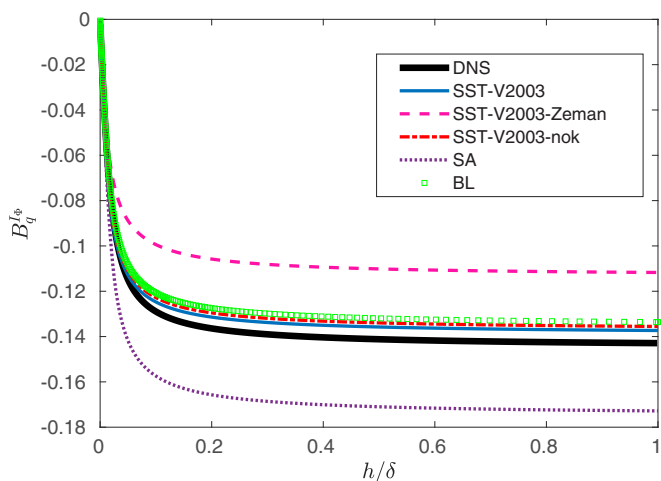


FIG. 8. Integrated contributions of the mean dissipation term (I_Φ) in the internal energy equation to the nondimensional wall heat flux, $\text{Re}_\tau = 1172$.

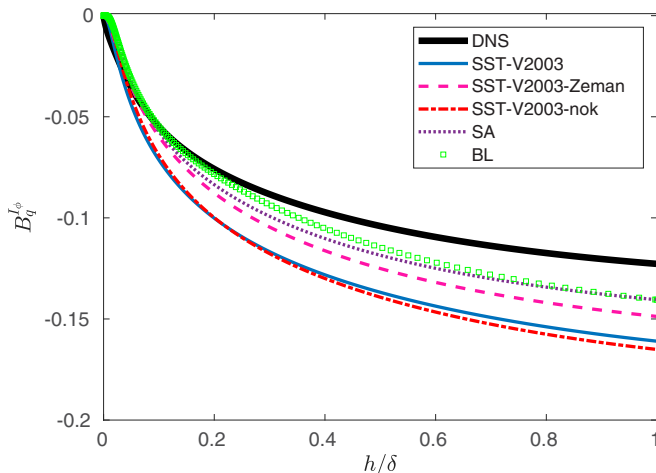


FIG. 9. Integrated contributions of the turbulent dissipation or apparent dissipation (I_ϕ) term in the internal energy equation to the non-dimensional wall heat flux, $Re_\tau = 1172$.

flux by 13.0% at $Re_\tau = 774$ and by 12.5% at $Re_\tau = 1172$. Figure 8 shows that the SA model has the largest negative contribution from mean dissipation of the models considered, and the magnitude of its apparent dissipation contribution is smaller than that of the SST-V2003-nok model. Overall, the BL model's contributions for these three terms agree the best with the DNS, suggesting that the historically good performance of this model for attached hypersonic boundary layers is not due to cancellation of errors, but rather because the energy balance generated by the model is relatively accurate, at least for a zero-pressure gradient, compressible boundary layer. The differences between RANS and DNS contributions to B_q for an integration height $h = \delta$ and $Re_\tau = 1172$ are given in Table II.

The integral analysis can also be used to display the net contribution of each term over the boundary layer as a function of Reynolds number, as in Fig. 10. Here, the contribution of the wall-normal turbulent heat flux to the wall heat flux for the RANS models is compared to DNS. The DNS contribution shows a slight decrease with Re_τ , which is replicated by the SA and BL models, while the SST model variants show a small increase with Re_τ . The BL model gives the best agreement with the DNS over this range of Reynolds numbers. In Fig. 11, the contributions of the mean and turbulent (or apparent) dissipation for the RANS models are compared to DNS. Each model captures the general trend of increasing mean dissipation contribution with Re_τ displayed by the DNS, although the DNS values are increasing more rapidly than the RANS models over the range of Re_τ considered, with the BL model coming closest to matching the slope of the

TABLE II. Difference between RANS B_q contribution and the DNS value, $Re_\tau = 1172$.

Mechanism	SST-V2003	SST-V2003-nok	SST-V2003-Zeman	SA	BL
Wall-normal turbulent heat transfer (I_{T_y})	+0.0160	+0.0187	+0.0020	+0.0224	+0.0030
Wall-normal mean convection (I_{C_y})	-0.0058	-0.0049	-0.0103	-0.0016	-0.0061
Stream-wise mean convection (I_{C_x})	+0.0087	+0.0084	+0.0106	+0.0094	+0.0093
Mean pressure dilatation ($I_{\dot{p}_1}$)	-0.0006	-0.0003	-0.0021	+0.0013	-0.0015
Turbulent dissipation (I_ϕ)	-0.0376	-0.0416	-0.0253	-0.0171	-0.0175
Mean dissipation (I_ϕ)	+0.0057	+0.0075	+0.0313	-0.0298	+0.0094
Total	-0.0129	-0.0116	+0.0072	-0.0126	+0.0019

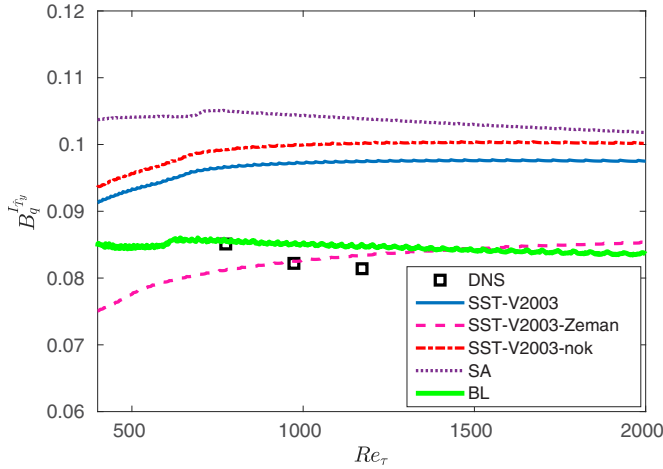


FIG. 10. Contribution of wall-normal turbulent heat flux (I_y) to wall heat flux vs friction Reynolds number.

DNS data. The SST-V2003 and BL models are closest to the DNS values over the range of Reynolds numbers considered. Also, neglect of k in the energy equation for the SST-V2003-nok model has little effect on the mean dissipation contribution. The Zeman compressibility correction diminishes the mean contribution across all Re_τ . The turbulent dissipation (or apparent dissipation for the SST-V2003-nok, SA, and BL models) for all models show the same trend of more negative contribution to the wall heat flux as Re_τ increases, although the BL gives a much shallower slope. This is in contrast with the DNS turbulent dissipation contribution, which stays nearly constant for the three points analyzed. This result points to the turbulent dissipation contribution as a possible source of deviation between DNS and RANS models for wall heat flux dependence on Reynolds number, particularly for the one- and two-equation models.

The mean dissipation contribution for the SST-V2003 model with and without compressibility correction is examined in more detail in Fig. 12, where the integrand for the mean dissipation contribution to wall heat flux coefficient is plotted in the near-wall region. The DNS results show that as Reynolds number increases, the magnitude of the contribution to the heat flux coefficient increases for $y/\delta < 0.1$, while it decreases for $y/\delta > 0.1$. This trend is more or less captured by both RANS models. The mean dissipation is somewhat overpredicted very near the wall by the

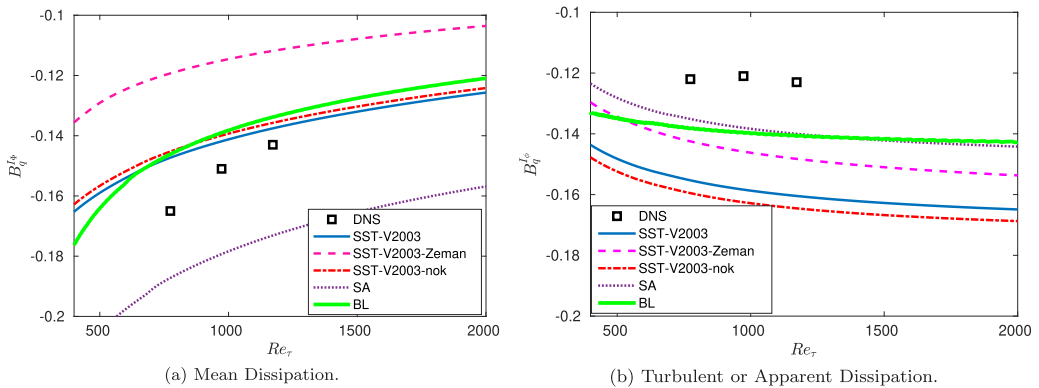


FIG. 11. Contribution of mean dissipation (I_ϕ) and turbulent or apparent dissipation (I_ϕ) to wall heat flux vs friction Reynolds number.

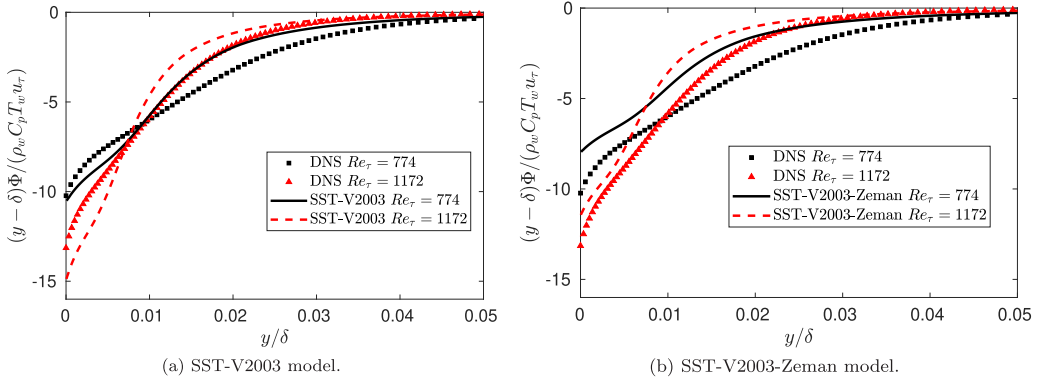


FIG. 12. Integrand for the mean dissipation contribution to wall heat flux ($h = \delta$).

SST-V2003 model, particularly for $Re_\tau = 1172$. This is consistent with the overprediction of wall shear stress at higher Reynolds numbers seen in Fig. 1, noting that $\Phi|_{y=0} \approx \mu_w (\frac{\partial U}{\partial y})^2|_{y=0} = \frac{\tau_w^2}{\mu}$. This error is partially compensated by the underprediction of the mean dissipation contribution further from the wall. The Zeman compressibility correction reduces the magnitude of the mean dissipation contribution to below the DNS value for all y . In this case, the compressibility correction overcorrects the contribution of the mean dissipation, which was very nearly correct for the original uncorrected model due to cancellation of errors just noted.

Figure 13 shows profiles of the turbulent dissipation ϕ , nondimensionalized using inner scales. The qualitative behavior of the RANS solutions and the DNS profiles is quite different, since the DNS profiles reach a peak at the wall, while the RANS turbulent dissipation is zero at the wall. This is an inherent behavior of the $k-\omega$ family of models without near-wall corrections. However, both the DNS and RANS profiles collapse for different Reynolds numbers using the inner scales for nondimensionalization. The Zeman compressibility correction is seen to increase the nondimensional dissipation over part of the boundary layer, due to its addition of a modeled dilational dissipation component. Figure 14 shows the integrands for the turbulent dissipation contribution to the wall heat flux coefficient. The DNS integrands exhibit modest changes going from $Re_\tau = 774$ to $Re_\tau = 1172$. Below $y/\delta \approx 0.05$, the integrand increases in magnitude while beyond y/δ the magnitude decreases; the sum of the two effects result in the overall flat contribution with Reynolds number noted in Fig. 11(b). The RANS solutions, on the other hand, show a marked increase in magnitude of the integrand for $y/\delta < 0.05$ with increasing Reynolds number. This is primarily due to the turbulent

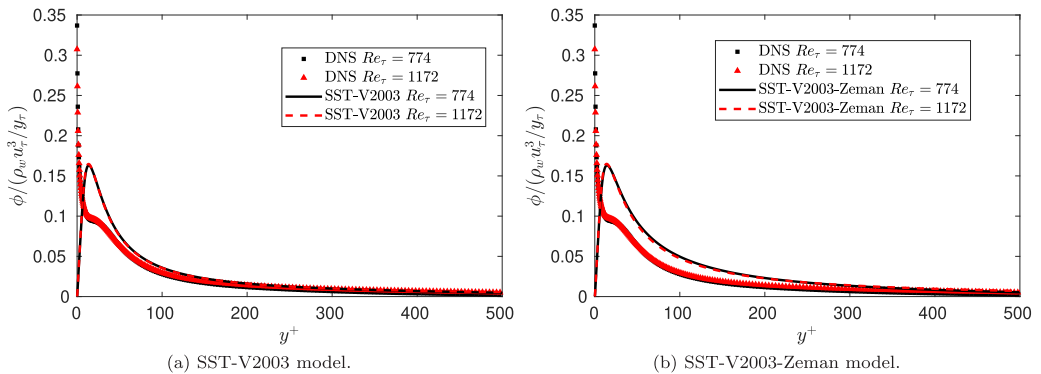


FIG. 13. Profiles of turbulent dissipation, nondimensionalized with inner scales ($y_\tau = \frac{\mu_w}{\rho_w u_\tau}$).

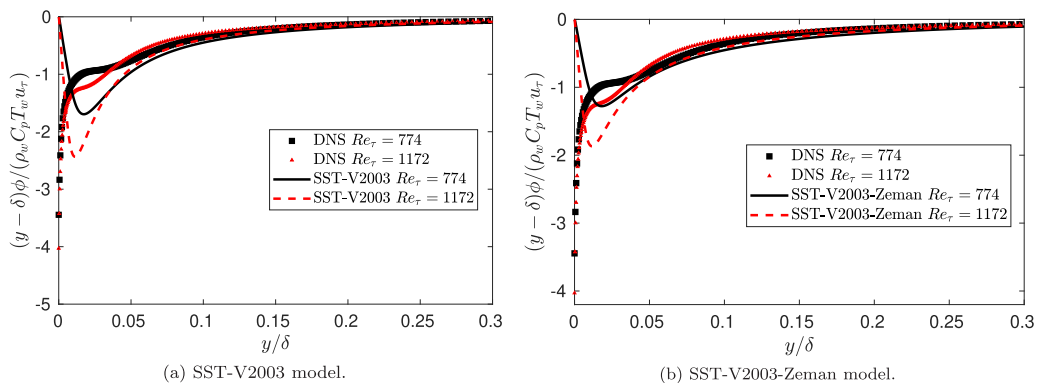


FIG. 14. Integrand for the turbulent dissipation contribution to wall heat flux ($h = \delta$).

dissipation scaling with the wall shear stress. The heat transfer coefficient is calculated using a mixed scaling with u_τ providing one velocity scale and $\sqrt{C_p T_w}$ another; this second scale is constant in the present flow. In the RANS solutions, the wall shear stress, and thus friction velocity, decrease at a slower rate with increasing Reynolds number than does the DNS. Therefore, the magnitude of the turbulent dissipation, which scales with u_τ^4 , is also decreasing more slowly than for the DNS. We conclude from these results that the issue with turbulent dissipation contribution to wall heat flux for the SST models is twofold: the inaccurate representation of the turbulent dissipation profile very close to the wall and the overprediction of wall shear stress with increasing Reynolds number.

VII. DISCUSSION

A few remarks are now provided on the utility and the limitations of the method developed in the previous sections for assessment of RANS models for aero-heating predictions in hypersonic flow. The present analysis provides information on how RANS models generate wall heat flux predictions, in particular, the role of different terms in the governing internal energy equation. This has been made possible by the recent availability of DNS solutions for hypersonic, cold-wall boundary layers. The conclusions drawn herein are specific to this particular flow, of course, although we expect many of them to generalize to other high Mach number, cold-wall attached boundary layers at other flow conditions. The performance of various RANS models in predicting the net contribution of terms in the internal energy balance has been assessed. Note, however, that the analysis does not directly lead to a remedy for any particular observed discrepancy in the model's predictions; for that, further analysis and sensitivity studies are required. The RANS solutions involve coupled mean momentum, temperature, and modeled fields, such that a "fix" to one of the terms can obviously effect one or more of the other involved terms. Nonetheless, the present analysis can be used to guide efforts to improve models and to assess the results of the attempted improvements. The analysis also leads to improved understanding of physical mechanisms involving the wall heat flux. For example, the decomposition of the contribution of the turbulent dissipation into various terms showed that the component of nonsolenoidal dissipation that resulted in the biggest impact to wall heat flux (ϕ_2) was different from the component that reached the highest peak magnitude in the boundary layer relative to the other components (ϕ_3).

The inspection of model mechanics through the lens of the integrated internal energy equation provides a means of understanding the precise impact of modeling assumptions on resulting wall heat flux predictions. For example, it was shown how neglecting to include the turbulence kinetic energy in the total energy equation leads to replacement of the turbulent dissipation with an apparent turbulent dissipation that is the negative of the modeled turbulence kinetic energy production term. The analysis also reveals the turbulent internal energy flux that is being modeled

in RANS, which includes a contribution from the term $\langle p \rangle \frac{\partial \langle u'_j \rangle}{\partial x_j}$. Terms that have previously been shown to be “small” for compressible, turbulent boundary layers, such as the pressure diffusion flux and pressure work, have been shown to be negligible in their effect on the wall heat flux, a perhaps useful distinction.

The three terms for which differences between RANS and DNS contributions to the wall heat flux resulted in potentially large errors in overall heat flux for the present flow were the wall normal turbulent heat flux, the mean dissipation, and the turbulent dissipation. The qualitative behavior of the turbulent heat flux contribution to wall heat flux was reasonable for the models considered, suggesting that the typical gradient diffusion closure used in all the models in this study is adequate. Quantitative differences in the contribution of this term to the wall heat flux may be down to specific differences in the eddy viscosity and mean temperature profiles generated by the different models, rather than a deficiency in the model form—although the constant turbulent Prandtl number assumption is known to be violated in boundary layers.

The magnitudes of the mean and turbulent dissipation contributions to wall heat flux appear to be the primary issues with the RANS models considered here. The mean dissipation depends primarily on generation of an accurate mean shear profile; none of the models considered here matched the DNS in this regard. However, with some fortuitous cancellation of error in the near-wall region, the SST-V2003 model accurately predicts the overall mean dissipation contribution well. In general, attempts to better approximate the mean velocity profile in the buffer region may lead to improved accuracy for this term.

Most models belonging to the $k - \omega$ family do not generate an accurate profile for turbulent dissipation close to the wall. This has not been a major issue, partly since it has not hampered predictive accuracy for quantities of interest such as skin friction and wall heating for lower speed flows, and partly since the modeled dissipation has traditionally been viewed as a quantity needed to supply a turbulence length scale for calculation of the eddy viscosity, rather than rigorously representing the small scale dissipation rate. This issue, however, was seen to cause an overshoot in the turbulent dissipation profile close to the wall and corresponding overprediction of the contribution of this term to the wall heat flux. We experimented with a low-Reynolds-number form of the SST model, described by Langtry and Sjolander [49]. This model is based on the low-Reynolds-number form described by Wilcox [22], which aims to allow both prediction of boundary layer transition as well as giving more correct asymptotic behavior of k and ϕ approaching a solid surface. We were able to obtain solutions with the low-Reynolds-number model which better approximated the near-wall behavior of turbulent dissipation; however, the improvement to wall heat flux predictions was only slight, due to persistent overprediction of the turbulent dissipation further from the wall. The widely used $k - \epsilon$ family of models, with associated low-Reynolds-number treatments, provide another path toward improvement of the near-wall turbulent dissipation behavior. Indeed, Prasad *et al.* [50] showed improved agreement of the Launder-Sharma $k - \epsilon$ model with DNS and experiment, relative to a $k - \omega$ model, for the present Mach 11 turbulent boundary layer case. However, $k - \epsilon$ models are known to have issues with capturing an accurate mean velocity profile in the logarithmic region of high Mach number boundary layers, which can adversely affect wall shear stress predictions [51].

While improving the modeling of turbulent dissipation may prove to be useful for heating predictions, another important issue is the improvement of the wall shear stress prediction. The overprediction of wall shear stress impacts both the mean dissipation and the turbulent dissipation, as discussed in Sec. VI. Since, for the RANS models, the wall shear stress appears to diminish more slowly with increasing Re_τ than the DNS, this likely also leads to incorrect variation of the wall heat flux with Re_τ . Figure 15 shows that the DNS Reynolds analogy factor, defined as $2C_h/C_f$, where $C_h = -q_w/[\rho_\infty U_\infty C_p (T_r - T_w)]$ is the Stanton number and $C_f = 2\tau_w/(\rho U_\infty^2)$ is the skin friction coefficient, varied slightly between 1.19 and 1.16 for this flow. The RANS models all predict a nearly constant factor of 1.19, demonstrating that the models are reproducing the correlation of mean wall heat flux with mean wall shear stress. Improvements to wall shear stress prediction for hypersonic, cold-wall boundary layers may involve sensitizing the closure to mean density gradients [51], accounting for density fluctuation correlations in the model for Reynolds stress, or both.

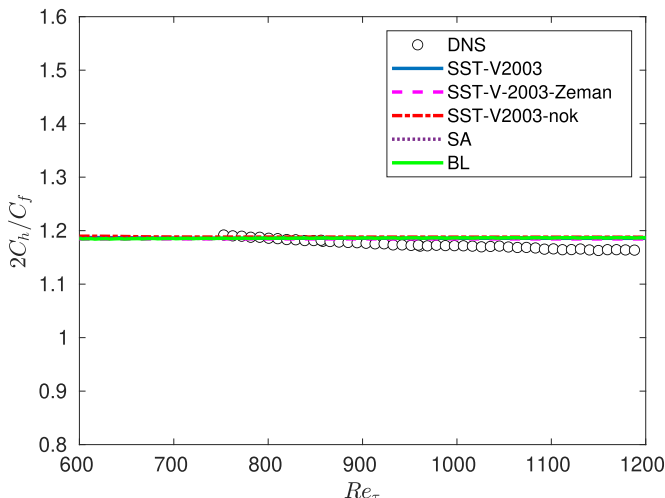


FIG. 15. Comparison of RANS model predictions of Reynolds analogy factor to DNS.

VIII. CONCLUSIONS

In this paper, we have demonstrated the following:

(1) The Reynolds-averaged internal energy equation and implied forms of this equation generated by various RANS modeling strategies provide a useful framework for analysis of RANS model aero-heating predictions.

(2) Integral relationships relating net effects of various terms in the averaged energy equation to the mean wall heat flux allow for identification of contributions of physical mechanisms and associated models to the wall heat flux, and provide a means to validate individual components of RANS models for prediction of wall heat flux, provided a suitable DNS database exists.

(3) Non-negligible contributions to the wall heat flux in a Mach 11 cold-wall turbulent boundary layer come from mean stream-wise and wall-normal convection, mean pressure dilatation, wall-normal turbulent heat flux, turbulent dissipation, and mean dissipation. Stream-wise and wall-normal molecular heat flux, stream-wise turbulent heat flux, and turbulent pressure dilatation are negligible contributors to wall heat flux for this flow.

(4) Neglect of turbulence kinetic energy in the RANS total energy equation implies that turbulent dissipation is approximated by the negative of turbulence kinetic energy production in the internal energy equation.

(5) The RANS models investigated herein give good predictions for the mean convection and mean pressure-dilatation contributions to wall heat flux, while they provide various levels of agreement on the remaining non-negligible components. The mean and turbulent dissipation components provide the most significant deviations from DNS, in general. The Zeman compressibility correction to the SST-V2003 model lowers the prediction of turbulent heat flux but does not improve overall agreement with the mean and turbulent dissipation components. The Baldwin-Lomax model gives the best agreement overall with the DNS; the relative success of the Baldwin-Lomax model is due to a more accurate internal energy balance generated by this model, at least for a zero-pressure gradient, cold-wall hypersonic turbulent boundary layer, rather than due to a fortuitous cancellation of errors.

(6) Inaccurate predictions of the turbulent dissipation contribution to wall heat flux for the models considered is due to both inaccurate near-wall turbulent dissipation profiles, as well as overprediction of the wall shear stress which results in overprediction of the turbulent dissipation magnitude.

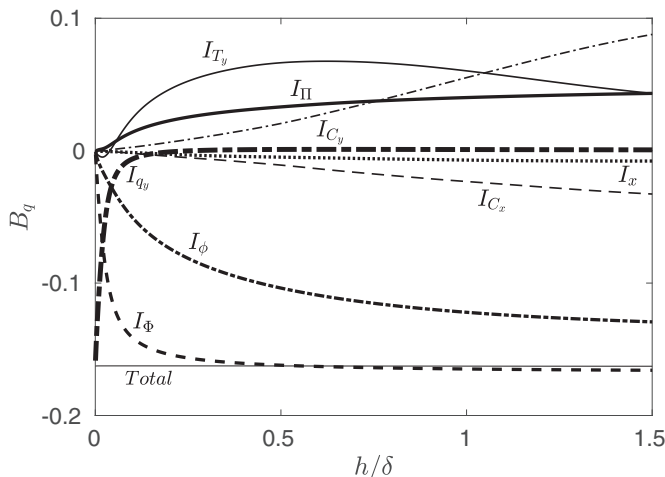


FIG. 16. Integrated contributions of terms in the internal energy equation to the nondimensional wall heat flux: DNS at $Re_\tau = 774$.

ACKNOWLEDGMENTS

Author Matthew Barone was supported by the Advanced Simulation and Computing Program, by the U.S. Department of Energy's National Nuclear Security Administration. Authors Gary Nicholson and Lian Duan were supported by the the Office of Naval Research (ONR) under Grant No. N00014-20-1-2261. The authors would also like to thank Dr. Junji Huang for his help with extracting some of the DNS profiles. Computational resources for computing the DNS data sets were provided by the DoD High Performance Computing Modernization Program and the Ohio Supercomputer Center. Sandia National Laboratories is a multimission laboratory managed and operated by National Technology & Engineering Solutions of Sandia, LLC, a wholly owned subsidiary of Honeywell International Inc., for the U.S. Department of Energy's National Nuclear Security Administration under Contract No. DE-NA0003525. This paper describes objective technical results and analysis. Any subjective views or opinions that might be expressed in the paper do not necessarily represent the views of the U.S. Department of Energy or the U.S. Government.

APPENDIX A: EFFECT OF UPPER INTEGRATION BOUND

Figure 16 shows the integrated contributions of terms in the internal energy equation with maximum upper integration bound increased to $h = 1.5\delta$. The qualitative behavior of the relative contributions does not change as the upper integration bound is extended beyond the boundary layer thickness [compare to Fig. 2(a)]. The mean and turbulent dissipation contributions are reaching asymptotic values. The wall-normal mean convection contribution continues to increase, since the mean wall-normal convective flux maintains a near constant value for an extended region outside of the boundary layer. This increase in wall-normal mean convection contribution is balanced by decreases in the stream-wise mean convection and wall-normal turbulent heat flux contributions.

APPENDIX B: TURBULENCE MODEL FORMS

1. SST-V2003 model functions and constants

The function F_2 appearing in the eddy viscosity formula (32) is

$$F_2 = \tanh(\arg_2^2), \quad \arg_2 = \max\left(2\frac{\sqrt{k}}{\beta^*\omega d}, \frac{500\mu(\{T\})}{\langle\rho\rangle d^2\omega}\right). \quad (\text{B1})$$

Each of the model constants is computed by blending an inner constant with subscript 1 with an outer constant with subscript 2:

$$C = F_1 C_1 + (1 - F_1) C_2. \quad (\text{B2})$$

The blending function F_1 is

$$F_1 = \tanh(\arg_1^4), \quad \arg_1 = \min \left[\max \left(\frac{\sqrt{k}}{\beta^* \omega d}, \frac{500 \mu(\{T\})}{\langle \rho \rangle d^2 \omega} \right), \frac{4 \langle \rho \rangle \sigma_{\omega 2} k}{CD_{k\omega} d^2} \right], \quad (\text{B3})$$

where

$$CD_{k\omega} = \max \left(2 \langle \rho \rangle \sigma_{\omega 2} \frac{1}{\omega} \frac{\partial k}{\partial x_j} \frac{\partial \omega}{\partial x_j}, 10^{-10} \right). \quad (\text{B4})$$

The model constants are

$$\begin{aligned} \gamma_1 &= \frac{5}{9}, & \gamma_2 &= 0.44, \\ \sigma_{k1} &= 0.85, & \sigma_{\omega 1} &= 0.5, & \beta_1 &= 0.075, \\ \sigma_{k2} &= 1.0, & \sigma_{\omega 2} &= 0.856, & \beta_2 &= 0.0828, \\ \beta^* &= 0.09, & \kappa &= 0.41, & a_1 &= 0.31. \end{aligned}$$

2. SA model functions and constants

The function f_w in (34) is

$$f_w = g \left(\frac{1 + c_{w3}^6}{g^6 + c_{w3}^6} \right)^{1/6}, \quad g = r + c_{w2}(r^6 - r), \quad r = \min \left(\frac{\check{v}}{\check{S} \kappa^2 d^2}, 10 \right). \quad (\text{B5})$$

The model constants are

$$\begin{aligned} c_{b1} &= 0.1355, & c_{b2} &= 0.622, & \sigma &= \frac{2}{3}, & \kappa &= 0.41, \\ c_{w1} &= \frac{c_{b1}}{\kappa^2} + \frac{1 + c_{b2}}{\sigma}, & c_{w2} &= 0.3, & c_{w3} &= 2, & c_{v1} &= 7.1. \end{aligned}$$

3. BL model functions and constants

The function F_{WAKE} is

$$F_{\text{WAKE}} = \min \left(y_{\text{MAX}} F_{\text{MAX}}, C_{\text{WK}} y_{\text{MAX}} \frac{u_{\text{dif}}^2}{F_{\text{MAX}}} \right), \quad (\text{B6})$$

where F_{MAX} and y_{MAX} are the maximum and argument of the maximum of the function

$$F(y) = y |\Omega| \left(1 - e^{-\frac{y}{A^+}} \right) \quad (\text{B7})$$

and

$$u_{\text{dif}} = \max(\sqrt{\{u_i\}\{u_i\}}) \quad (\text{B8})$$

with the maxima taken over each y profile. The function $F_{\text{KLEB}}(y)$ is

$$F_{\text{KLEB}}(y) = \left(1 + 5.5 \left[\frac{y C_{\text{KLEB}}}{y_{\text{MAX}}} \right]^6 \right)^{-1}. \quad (\text{B9})$$

The model constants are

$$\begin{aligned} k_l &= 0.4, & A^+ &= 26, & K &= 0.0168, & C_{\text{CP}} &= 1.6, \\ C_{\text{WK}} &= 1.0, & C_{\text{KLEB}} &= 0.3. \end{aligned}$$

- [1] O. J. H. Williams, D. Sahoo, M. L. Baumgartner, and A. J. Smits, Experiments on the structure and scaling of hypersonic turbulent boundary layers, *J. Fluid Mech.* **834**, 237 (2018).
- [2] M. MacLean, T. Wadhams, and M. Holden, Ground test studies of the HIFiRE-1 transition experiment. Part 2: Computational analysis, *J. Spacecr. Rockets* **45**, 1149 (2008).
- [3] R. J. Yentsch, D. V. Gaitonde, and R. Kimmel, Performance of turbulence modeling in simulation of the HIFiRE-1 flight test, *J. Spacecr. Rockets* **51**, 117 (2014).
- [4] P. A. Gnoffo, S. A. Berry, and J. W. V. Norman, Uncertainty assessments of hypersonic shock wave-turbulent boundary-layer interactions at compression corners, *J. Spacecr. Rockets* **50**, 69 (2013).
- [5] J. Huang, G. L. Nicholson, L. Duan, M. M. Choudhari, and R. D. W. Bowersox, Simulation and modeling of cold-wall hypersonic turbulent boundary layers on flat plate, *AIAA Scitech 2020 Forum, Orlando, FL* (AIAA, 2020), Paper No. 2020-0571,
- [6] T. T. Aiken, I. D. Boyd, J. Huang, and L. Duan, Assessment of Reynolds averaged Navier-Stokes models for a hypersonic cold-wall turbulent boundary layer, *AIAA Scitech 2022 Forum, San Diego, CA* (AIAA, 2022), Paper No. 2022-0586.
- [7] Z. Zhu, X. Zhang, X. Wang, and L. Zhang, Analysis of compressibility corrections for turbulence models in hypersonic boundary-layer applications, *J. Spacecr. Rockets* **57**, 364 (2020).
- [8] B. A. Bhutta and C. H. Lewis, Comparison of hypersonic experiments and PNS predictions. Part I: Aerothermodynamics, *J. Spacecr. Rockets* **28**, 376 (1991).
- [9] A. D. Dilley, Evaluation of CFD turbulent heating prediction techniques and comparison with hypersonic experimental data, Tech. Rep. NASA/CR-2001-210837, NASA, 2001.
- [10] C. L. Rumsey, Compressibility considerations for k - ω turbulence models in hypersonic boundary-layer applications, *J. Spacecr. Rockets* **47**, 11 (2010).
- [11] J. Huang, J.-V. Bretzke, and L. Duan, Assessment of turbulence models in a hypersonic cold-wall turbulent boundary layer, *Fluids* **4**, 37 (2019).
- [12] K. Fukagata, K. Iwamoto, and N. Kasagi, Contribution of Reynolds stress distribution to the skin friction in wall-bounded flows, *Phys. Fluids* **14**, L73 (2002).
- [13] W. H. Matthaeus, S. Oughton, and Y. Zhou, Contribution of Reynolds stress distribution to the skin friction in compressible turbulent channel flows, *Phys. Rev. E* **79**, 035401(R) (2009).
- [14] M. Yu, C.-X. Xu, and S. Pirozzoli, Genuine compressibility effects in wall-bounded turbulence, *Phys. Rev. Fluids* **4**, 123402 (2019).
- [15] K. Fukagata, K. Iwamoto, and N. Kasagi, Novel turbulence control strategy for simultaneously achieving friction drag reduction and heat transfer augmentation, in *Fourth International Symposium on Turbulence and Shear Flow Phenomena* (Begell House, New York, 2005), pp. 307–312.
- [16] A. Ebadi, F. Mehdi, and C. M. White, An exact integral method to evaluate wall heat flux in spatially developing two-dimensional wall-bounded flows, *Int. J. Heat Mass Transf.* **84**, 856 (2015).
- [17] P. Zhang and Z. Xia, Contribution of viscous stress work to wall heat flux in compressible turbulent channel flows, *Phys. Rev. E* **102**, 043107 (2020).
- [18] C. Wenzel, T. Gibis, and M. Kloker, About the influences of compressibility, heat transfer, and pressure gradients in compressible turbulent boundary layers, *J. Fluid Mech.* **930**, A1 (2022).
- [19] J. Huang, L. Duan, and M. M. Choudhari, Direct numerical simulation of hypersonic turbulent boundary layers: Effect of spatial evolution and Reynolds number, *J. Fluid Mech.* **937**, A3 (2022).
- [20] I. Pond, A. Ebadi, Y. Dubief, and C. M. White, An integral validation technique of RANS turbulence models, *Comput. Fluids* **149**, 150 (2017).
- [21] S. K. Lele, Compressibility effects on turbulence, *Annu. Rev. Fluid Mech.* **26**, 211 (1994).
- [22] D. C. Wilcox, *Turbulence Modeling for CFD*, 2nd ed. (DCW Industries, La Cañada, CA, 2002), p. 235.
- [23] E. R. van Driest, Turbulent boundary layer in compressible fluids, *J. Aeronaut. Sci.* **18**, 145 (1951).
- [24] R. D. W. Bowersox, Extension of equilibrium turbulent heat flux models to high-speed shear flows, *J. Fluid Mech.* **633**, 61 (2009).
- [25] R. D. W. Bowersox and S. W. North, Algebraic turbulent energy flux models for hypersonic shear flows, *Progr. Aerospace Sci.* **46**, 49 (2010).
- [26] N. Renard and S. Deck, A theoretical decomposition of mean skin friction generation into physical phenomena across the boundary layer, *J. Fluid Mech.* **790**, 339 (2016).

- [27] B. S. Baldwin and H. Lomax, Thin-layer approximation and algebraic model for separated turbulent flows, *16th Aerospace Sciences Meeting, Huntsville, AL* (AIAA, 1978), Paper No. 78-257.
- [28] P. R. Spalart and S. R. Allmaras, A one-equation turbulence model for aerodynamic flows, *Recherche Aérospatiale*, 5 (1994).
- [29] S. R. Allmaras, F. T. Johnson, and P. R. Spalart, Modifications and clarifications for the implementation of the Spalart-Allmaras turbulence model, *Proceedings of the 7th International Conference on Computational Fluid Dynamics (ICCFD7), Big Island, Hawaii* (2012).
- [30] F. R. Menter, M. Kuntz, and R. Langtry, Ten years of industrial experience with the SST turbulence model, in *Fourth International Symposium on Turbulence, Heat and Mass Transfer*, edited by K. Janjalic, Y. Nagano, and M. Tummers (Begell House, New York, 2003), pp. 625–632.
- [31] M. Howard, T. Fisher, M. Hoemmen, D. Dinzl, J. Overfelt, A. Bradley, K. Kim, and S. Rajamanickam, Employing multiple levels of parallelism for CFD at large scales on next generation high-performance computing platforms, *Proceedings of the Tenth International Conference on Computational Fluid Dynamics (ICCFD10), Barcelona, Spain* (2018).
- [32] S. L. Krist, R. T. Biedron, and C. L. Rumsey, CFL3D User’s Manual (ver. 5), *NASA Technical Memorandum NASA TM-1998-208444*, NASA (1998).
- [33] W. W. Liou and T.-H. Shih, On the basic equations for the second-order modeling of compressible turbulence, *NASA Technical Memorandum NASA-TM-105277*, NASA (1991).
- [34] O. Zeman, A new model for supersonic/hypersonic turbulent boundary layers, *31st Aerospace Sciences Meeting, Reno, NV* (AIAA, 1993), Paper No. 93-0897.
- [35] P. Gnoffo, S. Berry, and J. Van Norman, Uncertainty assessments of 2D and axisymmetric hypersonic shock wave-turbulent boundary layer interaction simulations at compression corners, *42nd AIAA Thermophysics Conference, Honolulu, Hawaii* (AIAA, 2011), Paper No. 2011-3142.
- [36] E. M. Taylor, M. Wu, and M. P. Martín, Optimization of nonlinear error for weighted essentially non-oscillatory methods in direct numerical simulations of compressible turbulence, *J. Comput. Phys.* **223**, 384 (2007).
- [37] M. Wu and M. P. Martín, Direct numerical simulation of supersonic turbulent boundary layer over a compression ramp, *AIAA J.* **45**, 879 (2007).
- [38] G.-S. Jiang and C.-W. Shu, Efficient implementation of weighted ENO schemes, *J. Comput. Phys.* **126**, 202 (1996).
- [39] J. Williamson, Low-storage Runge-Kutta schemes, *J. Comput. Phys.* **35**, 48 (1980).
- [40] L. Duan, I. Beekman, and M. Martín, Direct numerical simulation of hypersonic turbulent boundary layers. Part 2. Effect of wall temperature, *J. Fluid Mech.* **655**, 419 (2010).
- [41] L. Duan, I. Beekman, and M. Martín, Direct numerical simulation of hypersonic turbulent boundary layers. Part 3. Effect of Mach number, *J. Fluid Mech.* **672**, 245 (2011).
- [42] L. Duan, M. M. Choudhari, and M. Wu, Numerical study of acoustic radiation due to a supersonic turbulent boundary layer, *J. Fluid Mech.* **746**, 165 (2014).
- [43] L. Duan, M. M. Choudhari, and C. Zhang, Pressure fluctuations induced by a hypersonic turbulent boundary layer, *J. Fluid Mech.* **804**, 578 (2016).
- [44] C. Zhang, L. Duan, and M. M. Choudhari, Direct numerical simulation database for supersonic and hypersonic turbulent boundary layers, *AIAA J.* **56**, 4297 (2018).
- [45] M. A. Vyas, D. A. Yoder, and D. V. Gaitonde, Reynolds-stress budgets in an impinging shock-wave/boundary-layer interaction, *AIAA J.* **57**, 4698 (2019).
- [46] P. G. Huang, G. N. Coleman, and P. Bradshaw, Compressible turbulent channel flows: DNS results and modelling, *J. Fluid Mech.* **305**, 185 (1995).
- [47] P. J. Roache, *Verification and Validation in Computational Science and Engineering* (Hermosa, Socorro, New Mexico, 1998).
- [48] K. P. Griffin, L. Fu, and P. Moin, Velocity transformation for compressible wall-bounded turbulent flows with and without heat transfer, *Proc. Natl. Acad. Sci. USA* **118**, e2111144118 (2021).
- [49] R. B. Langtry and S. A. Sjolander, Prediction of transition for attached and separated shear layers in turbomachinery, *38th AIAA/ASME/SAE/ASEE Joint Propulsion Conference & Exhibit, Indianapolis, IN* (AIAA, 2002), Paper No. 2002-3641.

- [50] C. Prasad, M. Schwartz, and D. V. Gaitonde, A methodical assessment of two-equation turbulence models for high-speed flows, *AIAA Aviation 2021 Forum, Virtual Event* (AIAA, 2021), Paper No. 2021-2881.
- [51] P. G. Huang, P. Bradshaw, and T. J. Coakley, Assessment of closure coefficients for compressible-flow turbulence models, *NASA Technical Memorandum NASA-TM-103682*, NASA (1992).